# Development of Paint Stripe Testing Protocol

by

Ryan David Stevens

A Thesis Presented in Partial Fulfillment
of the Requirements for the Degree
Masters in Science

Approved April 2014 by the
Graduate Supervisory Committee:

B. Shane Underwood, Chair
Kamil Kaloush
Mike Mamlouk

ARIZONA STATE UNIVERSITY

May 2014

# ABSTRACT

Nighttime visibility of pavement markings is provided by glass beads embedded into the striping surface. The glass beads take light from the vehicle headlamps and reflect it back to the driver. This phenomenon is known as retroreflection. Literature suggests that the amount of the bead embedded into the striping surface has a profound impact on the intensity of the retroreflected light. In order to gain insight into how the glass beads provide retroreflection, an experiment was carried out to produce paint stripes with glass beads and measure the retroreflection. Samples were created at various application rates and embedment depths, in an attempt to verify the optimal embedment and observe the effect of application rate on retroreflection. The experiment was conducted using large, airport quality beads and small, road quality beads. Image analysis was used to calculate the degree to which beads were embedded and in an attempt to quantify bead distribution on the stripe surface. The results from the large beads showed that retroreflection was maximized when the beads were embedded approximately seventy percent by bead volume. The results also showed that as the application rate increased, the retroreflection increased, up to a point and then decreased. A model was developed to estimate the retroreflectivity given the amount of beads, bead spacing, and distribution of bead embedment. Results from the small beads were less conclusive, but did demonstrate that the larger beads are better at providing retroreflection. Avenues for future work in this area were identified as the experiment was conducted.

DEDICATION

For my grandparents.

ACKNOWLEDGMENTS

I would first and foremost like to acknowledge Dr. Shane Underwood for his leadership and support during my graduate career. Without his guidance, this research could not have been possible. Secondly, I would like to thank the rest of my thesis committee, Dr. Kamil Kaloush and Dr. Mike Mamlouk for teaching me so much throughout both my graduate and undergraduate studies. I would like to acknowledge Ms. Maria Elena De la Cruz, Mr. Frank Himpsl, and Mr. Jeff Faulkner from the Arizona Department of Transportation for lending me the equipment necessary to conduct this research. I'd like to thank the all the graduate students in the Pavement Analysis Research Group at Arizona State University for their support and assistance throughout this research. Finally, I'd like to acknowledge Mr. Rhett Butler for bringing the importance of retroreflectivity to the attention of the pavement analysis research group at Arizona State University.

TABLE OF CONTENTS

CHAPTER Page

LIST OF FIGURES

FIGURE Page

FIGURE Page

LIST OF TABLES

TABLE Page

# Chapter 1 Introduction

It has been estimated that sixty percent of all highway fatalities are a result of lane departures [1]. Pavement markings are critical in establishing lane awareness and decreasing lane departure incidents. A particular concern regarding pavement markings is nighttime visibility. In order to provide improved nighttime visibility for vehicle operators, glass beads are embedded into the surface of pavement marking materials. The glass beads provide retroreflectivity to the pavement markings. Retroreflectivity is the optical phenomenon in which light reflects off of a surface back to its source. Pavement markings use retroreflection to reflect light from the vehicle headlights backwards to the driver, providing increased visibility.

The overall objective of this study was to gain insight into the specifics of glass bead application which affect the retroreflection of the overall striping. The study aimed to show the relationship between the percent of the bead volume embedded in the striping and the retroreflection of the stripe by using laboratory produced stripes, which incorporated drop-on glass beads,. Various studies have suggested that the optimal embedment range is between fifty and sixty-five percent. Striping samples were made in a laboratory setting with glass beads dropped on the stripe at various application rates and embedment depths. Two sizes of beads were used in sample production in order to observe the difference between airport and road quality beads.

The remainder of this document is presented in four chapters. Chapter 2 provides a literature review, which forms the basis of this research. It discusses concepts related to pavement striping materials, reflection characteristics, and retroreflective glass beads. It

also provides a brief overview of work related to retroreflectivity degradation. Chapter 3 describes the methodology of experimentation including the construction of the paint stripe production apparatus, image analysis, and the production of samples for analysis. Chapter 4 provides the results of sample production and discusses insights gained from the results and analysis. Chapter 5 provides a summary of results, discusses limitations of the experiment, and suggests opportunities for future work.

# Chapter 2 Literature Review

## 2.1 Pavement Marking Materials

A variety of materials are used to delineate the travel lanes on roadways including paints, thermoplastics, and other special materials. These materials can be classified in two ways: durable and non-durable. In general, paint based materials are considered non-durable; most other materials are considered durable [1]. Water-based paints and thermoplastics are the most commonly used delineation materials by transportation agencies [2].The accompanying sub-sections provide a brief overview of common striping materials.

### *2.1.1 Water-Based Paint*

Water-based paints are the most common delineation materials in use today [4]. Water-based paints are widely used because of the relative ease of application and lower cost compared to other materials. Water-based paints are suitable for both portland cement concrete (PCC) and asphalt concrete (AC). Water-based paints often have a short drying time, which allows for the re-opening of traffic to the roadway within a few minutes after the paint is applied. One big drawback to the use of water-based paint is the service life, which is generally accepted to be less than one year [4]. The actual service life is dependent of a variety of factors such as the amount of vehicle traffic and climatic conditions, but ranges from six months to two years [4].

### *2.1.2 Thermoplastic*

Thermoplastic is the second-most used delineation material. Although more expensive and more difficult to install when compared to paints, the extension in service

life helps balance the overall cost to a transportation agency [4]. In general, thermoplastic markings have a three to five year service life [4]. Thermoplastics can be used on both PCC and AC; however, environmental conditions such as temperature and moisture may limit the ability of thermoplastic to adhere to the pavement surface. Since thermoplastics have a greater thickness than paint, in general, substantial damage may be incurred on thermoplastic delineation during snow plow operations [4].

### *2.1.3 Preformed Tape Markings*

Preformed movement markings can be used in a variety of applications ranging from continuous striping, temporary line diversions, crosswalks, and special markings such as arrows or words. Preformed tapes can be used in a permanent or temporary capacity. Temporary tapes are typically pre-coated with an adhesive for easy installation. Permanent tape markings may have a stronger adhesive coating or may be heated to create a thermal bond with the pavement surface. On freshly installed or rehabilitated AC pavements, the tape can be inlaid into the pavement surface. If the AC is still warm, the tape can be rolled onto the pavement with a steel drum during the final rolling of the pavement surface. The tape markings may also be overlaid onto the pavement surface on older, existing pavements. Preformed tape markings may be used temporarily, but can also last up to four years given proper installation [4].

### *2.1.4 Epoxy*

Epoxy markings are durable on both PCC and AC pavement surfaces. Epoxy markings are typically two-component materials. The exceptional durability is a result of the superior bonding to the pavement surfaces which results from the chemical reactions

which occur when the two components are mixed. Epoxy markings, however, require a substantial amount of time to cure to the pavement surface. Some epoxy markings can take up to forty minutes to cure [4]. One of the benefits of using epoxy markings is that epoxy markings can be applied to the pavement surface at surface temperatures as low as thirty-five degrees Fahrenheit.

## 2.2 Optics

When discussing the visibility of pavement markings, it is important to have a basic understanding how light works in the context of pavement markings. Optics is the branch of physics which involves the behavior of light and the interaction between light and matter. In this document, 'light' refers to the wavelengths of the visible spectrum. When light interacts with matter, two outcomes are possible: reflection and refraction. When the eye sees an object, it takes in light, which has been reflected off of the object. The two types of reflection of interest in this thesis are diffuse and specular reflection. When light strikes a transparent object, it can be distorted through refraction. The amount of refraction experienced by the light is dependent on the material composition.

### *2.2.1 Reflection*

Light can reflect off a surface in three different ways: specular reflection, diffuse reflection, and retroreflection. Specular reflection occurs when light hits a surface with a particular entrance angle and leaves the surface with an equal exit angle. An example of this type of reflection would be a laser reflecting off of a mirrored surface. Diffuse reflection occurs when the light source hits a surface and is reflected in a variety of directions. The micro-texture of the surface causes the light to reflect in a variety of exit

angles which often differ from the entrance angle. Retroreflection is the phenomenon of the light hitting a surface and being redirected back to its source. For pavement markings, retroreflection is desired for nighttime visibility, particularly for roads with no external illumination, so that car headlights illuminate the striping and allow for increased visibility. Figure 2-1 illustrates the three types of reflection. Glass beads, which are described in Section 2.3, are used to provide nighttime visibility by reflecting the light from vehicle headlights.

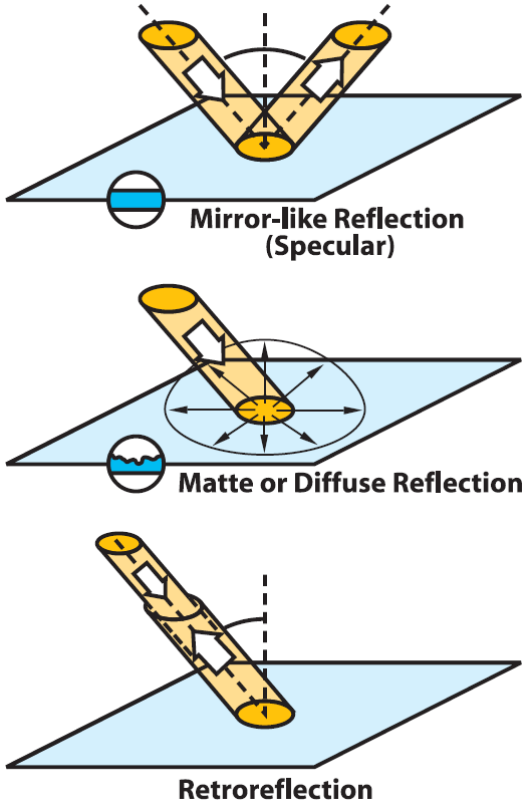


Figure 2-1: Three Types of Reflection [5]

*2.2.2 Retroreflection*

No matter which delineation material is used, a critical aspect of the delineation's nighttime effectiveness comes from retroreflectivity. The Manual on Uniform Traffic Control Devices (MUTCD) defines retroreflectivity as, "a property of a surface that allows a large portion of the light coming from a point source to be returned directly back to a point near its origin" [6]. For lane delineation, retroreflectivity is quantified by the coefficient of retroreflected luminance (RL), which is measured in millicandelas per meter squared of luminance (mcd/$m^2$/lux). The American Society for Testing Materials (ASTM) standard number E1710 specifies that the 30-meter geometry be used when evaluating the retroreflectivity of pavement delineations [7]. The 30-meter geometry measures retroreflectivity of a point that is thirty meters away from of the light source, and is schematically diagrammed in Figure 2-2. This geometry was used in a test procedure developed by The European Committee for Standardization (CEN) for measuring the retroreflection of pavement marking under dry conditions; the test procedure was subsequently adopted by ASTM [8]. The study assumed that the distance the driver could see at night was 30 meters [1].

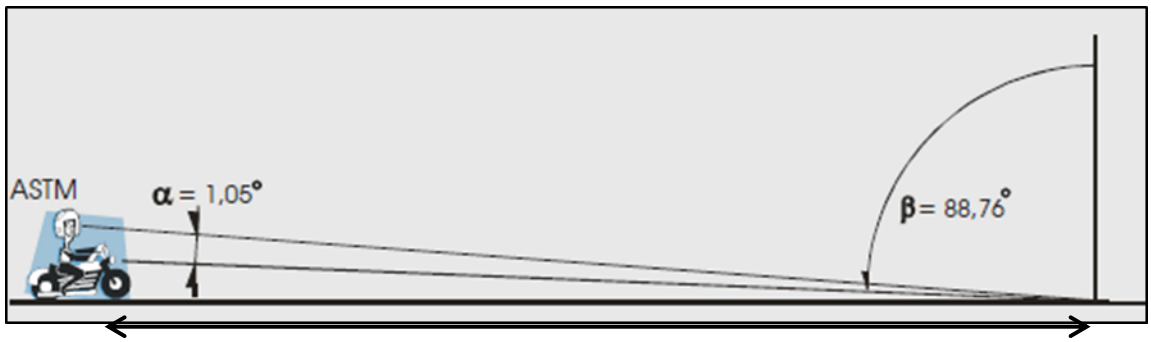


Figure 2-2: 30-meter Geometry [9]

In 2010, the FHWA released proposed guidelines for minimum retroreflectivity standards for pavement markings. Until the FHWA released its proposed guidelines, researchers had used a wide range of retroreflectivity values for the purpose of modeling the degradation of retroreflectivity for various markings. As a result, there is significant variation between the estimated service lives of pavement markings, because each study used a different retroreflectivity value to determine the point at which the marking was no longer useful. Table 2.1 shows the proposed minimum retroreflectivity values proposed by the Federal Highway Administration. It is noted that according to Bahar et al, participants in a visibility study gave high visibility ratings to markings with retroreflectivity values greater than one hundred [10].

Table 2.1: Proposed Minimum Retroreflectivity Values for Longitudinal Markings [1]

| | Posted Speed (mph) | | |
|---|---|---|---|
| | ≤ 30 | 35-50 | ≥ 55 |
| Two-lane roads with center line markings only | n/a | 100 | 250 |
| All other roads | n/a | 50 | 100 |

## 2.3 Reflective Glass Beads

Reflective glass beads are critical for providing non-raised, horizontal pavement markings with proper retroreflection. Beads are classified by their size and gradation into five categories [6]. By convention, Type I and Type II beads are referred to as ‘standard beads’ while the other three types are considered to be ‘large beads’ [1]. Within each type, the beads range in size. The specific gradation of bead sizes allows the marking to achieve a higher bead density and the proper depth of embedment. The typical bead size gradations for each bead type are presented in Table 2.2 and demonstrated in Figure 2-3: Bead Types I-V Typical Size Gradation. In general, Type I and Type II are considered

‘standard beads’ used in roadway applications, while Type III, Type IV, and Type V beads are considered ‘large beads’ and are typically used in airport applications.

Table 2.2: Typical Bead Size Gradations - After [3]

| **US Sieve Size** | **Sieve Size mm.** | **Mass Percent Passing** | | | | |
|---|---|---|---|---|---|---|
| | | **Type I** | **Type II** | **Type III** | **Type IV** | **Type V** |
| No.8 | 2.380 | - | - | - | - | 100 |
| No.10 | 1.999 | - | - | - | 100 | 95-100 |
| No.12 | 1.679 | - | - | 100 | 95-100 | 80-95 |
| No.14 | 1.410 | - | - | 95-100 | 80-95 | 10-40 |
| No.16 | 1.191 | 100 | - | 80-95 | 10-40 | 0-5 |
| No.18 | 1.001 | - | - | 10-40 | 0-5 | 0-2 |
| No.20 | 0.848 | 95-100 | - | 0-5 | 0-2 | - |
| No.25 | 0.706 | - | - | 0-2 | - | - |
| No.30 | 0.594 | 75-95 | 100 | - | - | - |
| No.40 | 0.419 | - | 90-100 | - | - | - |
| No.50 | 0.297 | 15-35 | 50-75 | - | - | - |
| No.80 | 0.178 | - | 0-5 | - | - | - |
| No.100 | 0.150 | 0-5 | - | - | - | - |

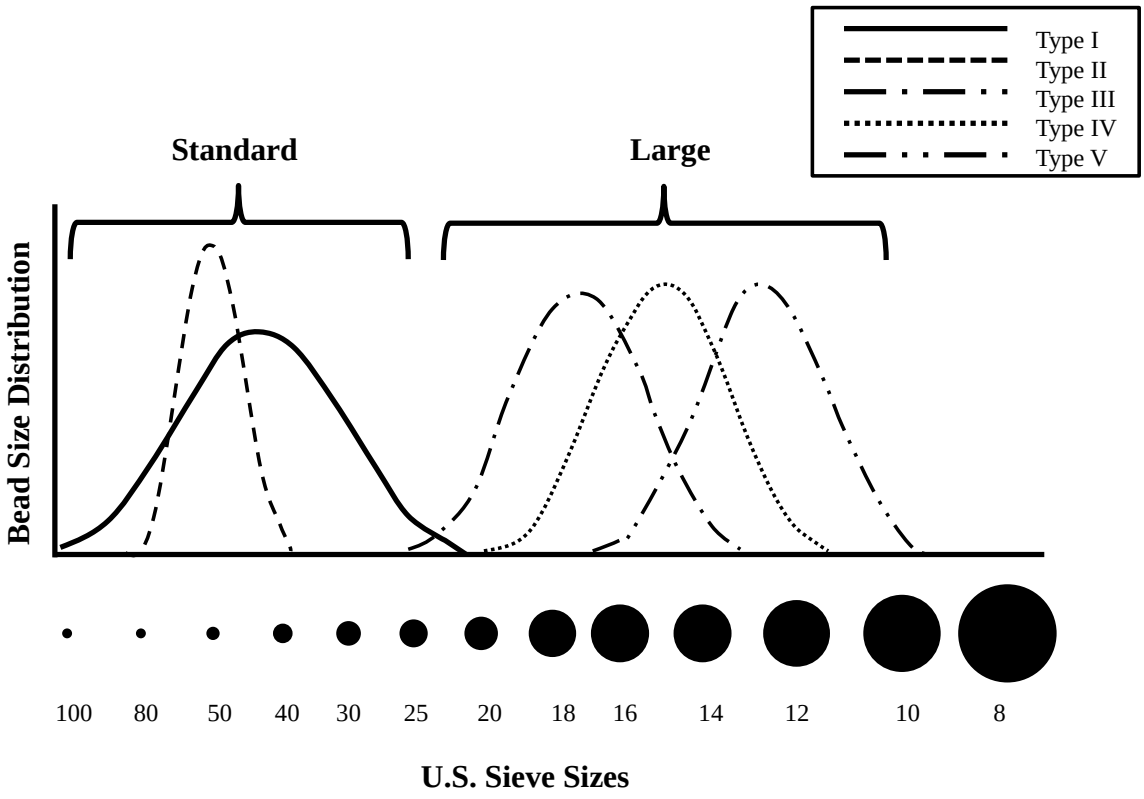


Figure 2-3: Bead Types I-V Typical Size Gradation – After [3]

For lane delineation markings, retroreflectivity is provided by the embedment of glass beads into the surface of the material. When light from the headlights of a vehicle enters a bead on the material's surface, the light is refracted inside the bead, reflects off of the marking material on the underside of the bead, and is refracted again through the bead before finally exiting the bead on a trajectory that is similar to the trajectory through which it entered. This phenomenon is demonstrated in Figure 2-4.

### *2.3.1 Contribution of Specular Reflection to Retroreflection*

The glass beads use specular reflection in the process of providing retroreflection. Some light which reaches the glass bead is lost due to specular reflection at the first interaction with the bead surface. Once light enters the bead, it is bent by refraction, hits

the far side of the bead, and is some is reflected back by specular reflection, although most is refracted out of the glass bead. This phenomenon is demonstrated in Figure 2-4. Although the light can reflect specularly within the bead, two things can happen when specular reflection is considered alone: the light will not exit the bead, or the light exits the bead at an angle which does not assist the driver [11].

### *2.3.2 Contribution of Refraction and Diffuse Reflection to Retroreflection*

When light transitions from one medium to another, it is often bent or distorted. This phenomenon is known as diffraction. The amount of diffraction is dependent on a material property known as the refractive index. Snell's Law, shown in Equation (2.1) relates the angle of refraction to the refractive indices of the two media as:

$$n_0 \sin i = n_1 \sin r \qquad (2.1)$$

where $n_0$ is the refractive index of the initial medium, $n_1$ is the refractive index of the medium in question, $i$ is the incident angle, and $r$ is the angle of refraction. Air has an index of refraction slightly greater than one at standard temperature and pressure. Many analyses of refractive angles assume air's refractive index as equal to one. Typically, the glass beads used in pavement striping are specified to have a refractive index of at least 1.5 [12].

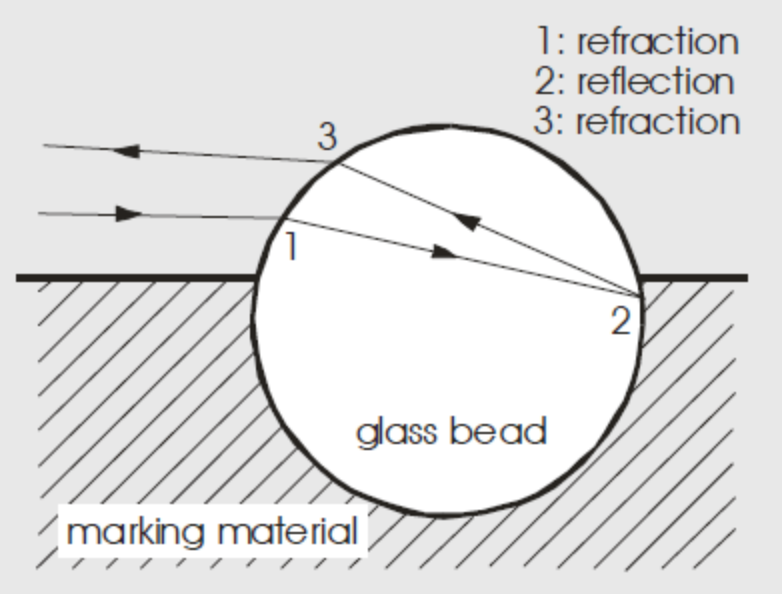


Figure 2-4: Retroreflection within a Glass Bead [9]

The efficiency of retroreflectivity is dependent on a number of factors such as bead embedment depth, bead size, density on the paint surface, roundness, the optical properties of the paint itself, and the refractive index of the glass bead [13]. A study conducted by Grosges analyzed the retroreflection of glass beads on paint striping. Figure 2-5 simulates the paths of light for a bead embedded sixty percent into the paint film. The effective contribution of retroreflection comes from the diffusion cone. Although the majority of the emitted rays in Figure 2-5 seem to exit the bead at angles which would not be conducive to retroreflectivity, Grosges explained that actual retroreflected light comes from the diffusion cone. Grosges also remarked that the major portion of light flux constituted light continuing forward (increasing x position in Figure 2-5) and was essentially induced by specular reflections within the bead. The retroreflected portions of the light flux was provided by the non-directional, diffuse reflection at the back of the bead and exited through the diffusion cone [13].

The embedment depth plays a crucial role in the efficiency of this retroreflection. Grosges conducted an experiment to evaluate the intensity of the retroreflection at various embedment depths. He determined that the intensity of retroreflection is maximized when the bead is embedded approximately between sixty and sixty-five percent [13]. The variation of retroreflection intensity is shown in Figure 2-6.

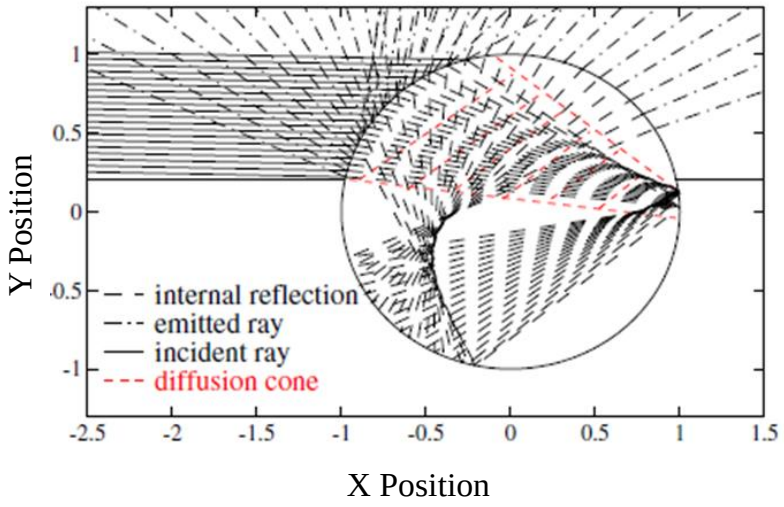


Figure 2-5: Ray Tracing Representation of Light Refraction in a Glass Bead at Sixty Percent Embedment [13]

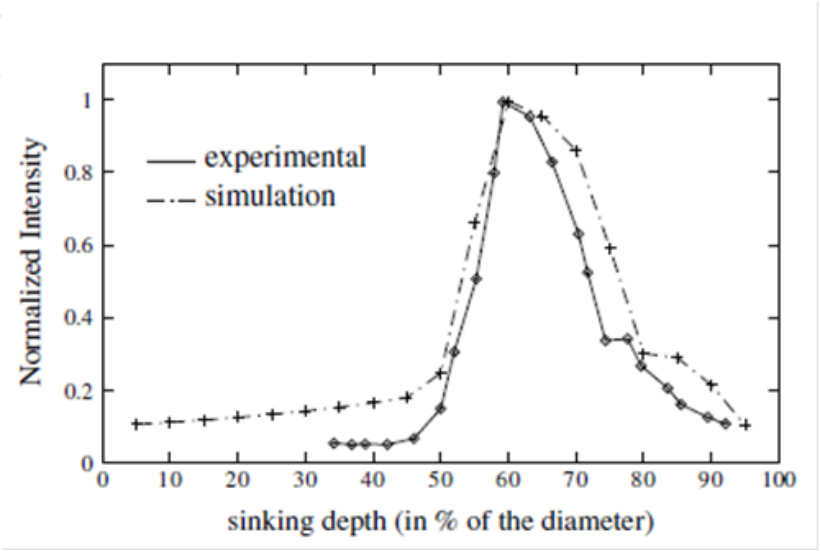


Figure 2-6: Single Bead Retroreflection Intensity vs. Embedment Percentage [13].

As demonstrated by Grosges, in order to attain the optimum retroreflectivity, beads should be embedded approximately sixty-five percent [13]. If beads are exposed less than the optimum depth, the longevity of the beads effectiveness can be reduced. If beads are over-embedded the retroreflectivity is reduced. An important contributor to the bead embedment is the thickness of the marking and the size of the bead. The bead size gradation helps ensure that the majority of beads can achieve the desired embedment even with fluctuations in the marking thickness. Paints are typically between fifteen and twenty-five mils thick, while thermoplastics can have a range of ninety to one hundred twenty mils. Smaller beads may be more likely to become over-embedded if the thickness of the marking is too large. Alternatively, large beads may be under-embedded if the marking thickness is too small. This demonstrates the importance of using the correct sized bead for the specific marking material.

## 2.4 Glass Bead Application

Glass bead applied to pavement markings are applied to the markings at the time of installation. One vehicle is used to both apply the marking and embed the glass beads as the vehicle travels along the pavement. Beads are either dropped onto the marking or are sprayed onto the marking. Although paint thickness and bead application rate are specified by state marking standards, these parameters are often difficult to control in the field, and the overall quality of the stripe is dependent on the experience of the crew installing the marking [1]. Technicians evaluate the amount of beads deposited onto a stipe with a magnifying glass and adjust the application of the beads until the desired bead density is achieved. A striping vehicle applying glass beads is shown in Figure 2-7 and Figure 2-8.

Figure 2-7: Striping Vehicle Applying Glass Beads with Spray Nozzles [14]

Figure 2-8: Application of Striping and Glass Beads Over Existing Marking [14]

In order to ensure proper bead coverage, excess beads are applied to the stripe and a level of overspill is accepted as industry practice. The low cost of the beads makes more precise application of beads or recovery of excess beads uneconomical [14].

## 2.5 Retroreflection Degradation Models

Initial retroreflectivity is only one component in evaluating service life of pavement markings. Various studies have examined the degradation of the retroreflectivity of in

service pavement striping. The degradation of retroreflection can be influenced by many factors including:

- Material Type
- Geographic location
- Climate
- Traffic volume
- Percent heavy trucks
- Pavement material type
- Quality of application

The loss of retroreflection is a key determinant of a pavement marking's service life. Numerous models have been developed in order to predict the loss of retroreflection. Most of the models predict retroreflectivity as a function of initial retroreflectivity, traffic characteristics, and the age of the markings. A study conducted by the Alabama Department of Transportation (ALDOT) conducted a study to examine various degradation models in order to determine which model, if any would represent the data observed in Alabama. The study found that two models could be used, but that extrapolation beyond the available data resulted in service lives over twice that of typical thermoplastic markings and occasionally greater that typical pavement service life as high as 20 years [15]. The study noted that Alabama had geographical and climatic conditions which differed from the conditions present where the models were developed.

Thamizharasan et al [15], [16] found that new markings can experience an increase in retroreflectivity before experiencing a decrease over time. As new pavement markings were exposed to traffic, some of the marking was worn off which exposed the

more of the beads. As the beads were exposed and paint worn off, the number of beads at sixty percent embedment increased. After this increase, bead loss and the wearing down of the markings resulted in a decreasing retroreflectivity. This predictive model is shown in Figure 2-9. Much older markings exhibited an almost linear degradation over time. The degradation trend of existing striping is shown in Figure 2-10.

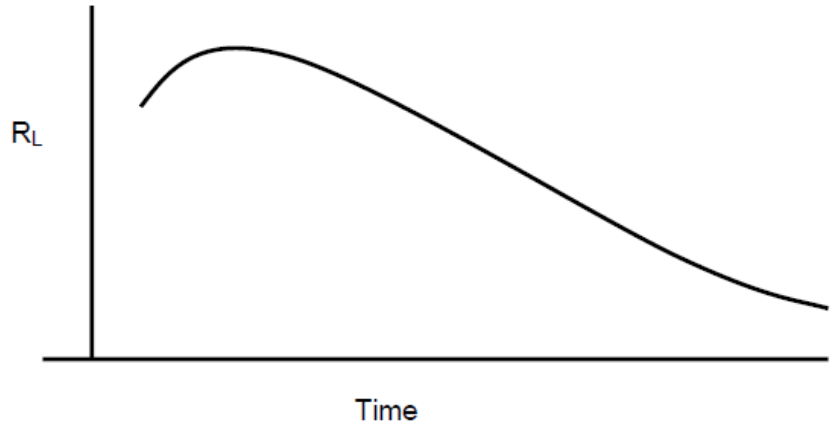


Figure 2-9: New Pavement Marking Retroreflection Degradation Trend [1]

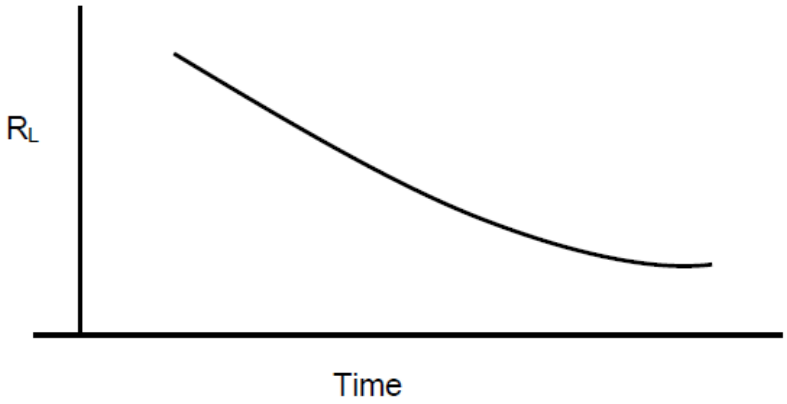


Figure 2-10: Existing Pavement Marking Retroreflection Degradation Trend [1]

# Chapter 3 Methodology

In order to gain insight into the effects of adding glass beads to pavement markings, it was decided that stripes should be made in a laboratory environment. Additionally, it was decided that some analysis metrics would be needed in order to characterize the arrangement of beads on the paint surface. To that end, image analysis was used to interpret the laboratory stripes in an attempt to quantify the bead distribution characteristics and see if a correlation existed between these metrics and retroreflection. The experimental study presented in this document was divided into three distinct phases:

1. Design, construct, test, and refine a laboratory apparatus to create paint stripes. Then fabricate initial samples to develop stripe evaluation metrics and to properly produce the samples.
2. Create and experiment on paint stripes containing airport quality beads to quantify the independent and interactive effects of application rate and embedment depths.
3. Create and experiment on paint stripes with road quality beads to verify the findings from phase 2 and identify any additional interactions between rate, depth, and bead type.

## 3.1 Phase I: Building Apparatus and Pilot Study

Phase I consisted of the construction of the apparatus, testing of pre-production striping samples, and defining appropriate evaluation metrics. After the apparatus was constructed, airport quality beads were used to fabricate stripe samples, which were subsequently examined. Through this examination, the metrics for evaluation were developed.

### *3.1.1 Development of Bead Drop Apparatus*

In order to evaluate the glass beads, it was decided that the beads should be tested on a suitable marking material. Although glass beads are often used in thermoplastic and paint, it was decided that water-based, latex, traffic paint would be the best media on which to evaluate the beads. The paint could be applied at room temperature, which made it easier to work with compared to thermoplastic. Thermoplastic would need to be applied at a high temperature, which made the use of thermoplastic impractical for this experiment. Additionally, since the aim of the experiment was to evaluate the retroreflection of glass beads applied to pavement markings, paint was a simple, easy to handle marking material which could be used to evaluate the effect of the beads. The experiment was not intended to test different colors or materials, so white traffic paint was used throughout the three phases.

Prior to the construction of the bead drop box apparatus, the critical functions were defined. First, the apparatus would need to provide a suitable base on which to carefully apply the paint to a glass substrate. Second, a mesh box would be needed to evenly distribute the gravity-dropped beads. Finally, the dropper mechanism needed to hold the beads until the paint stripe below was prepared. The dropping of the beads simulates, but does not replicate, the process of the striping truck applying the beads to the surface. The apparatus that was constructed was based on the device developed during NCHRP Project 4-38 [18]. The apparatus consists of three components: a base on which the paint can be applied to a glass plate; a mesh box through which the beads are dropped onto the stripe; and a drawdown blade to create paint stripes of uniform thickness.

Base

The base of the apparatus was made of 3/4″ plywood. Along the sides of the base, plywood strips were attached and positioned with an appropriately spaced gap so that the resulting lip would hold the glass plate in place. The strips also served as a guide for the drawdown blade (described in more detail below). The path of the drawdown blade was 4″ wide. The base of the apparatus is show in Figure 3-1.

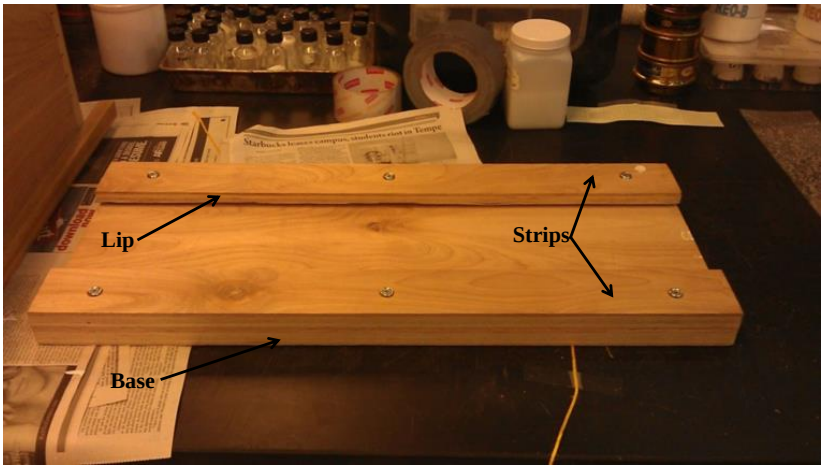


Figure 3-1: Base of Apparatus

Drop Box

The drop box component of the apparatus was made from ¾″ plywood and a combination of multiple ¼″ square mesh wire. The dimensions of the box are approximately 5 ½″ x 19 ½″ x 14″ with ten layers of the ¼″ wire mesh vertically separated by 1″. The drop box produces a stripe 4″ wide with beads covering an 18″ length of striping. The wire mesh screens are oriented in an alternating 90 degree and 45 degree orientations to facilitate an even bead distribution. The mesh orientation is shown in Figure 3-2. Various views of the drop box are shown in Figure 3-3.

During the apparatus development and shakedown process, beads were dropped through the box onto adhesive tape to make rapid observations on how well or poorly the

apparatus could produce an evenly distributed stripe. From the drops on the adhesive tape, it was observed qualitatively that when the beads were more evenly distributed at the top of the box a better distribution resulted on the adhesive tape. This observation lead to the development of a bead dropper that would be attached to the top of the box. The goal for this component of the apparatus was to drop the beads vertically through the box without any spinning or directional movement. From trials it was found that dropping the beads via a spinning dropper could lead to segregation across the stripe width. The dropper mechanism is shown in Figure 3-5. The dropper itself was constructed from aluminum and designed with springs to hold the dropper closed until the operator squeezed the dropper and released the beads. To ensure that an even distribution along the dropper length was achieved, straight horizontal lines were scribed on both interior sides of the dropper along the entire length. The heights of these lines were established based on calculation of the approximate loading rates and assumptions of the packing density of spherical beads.

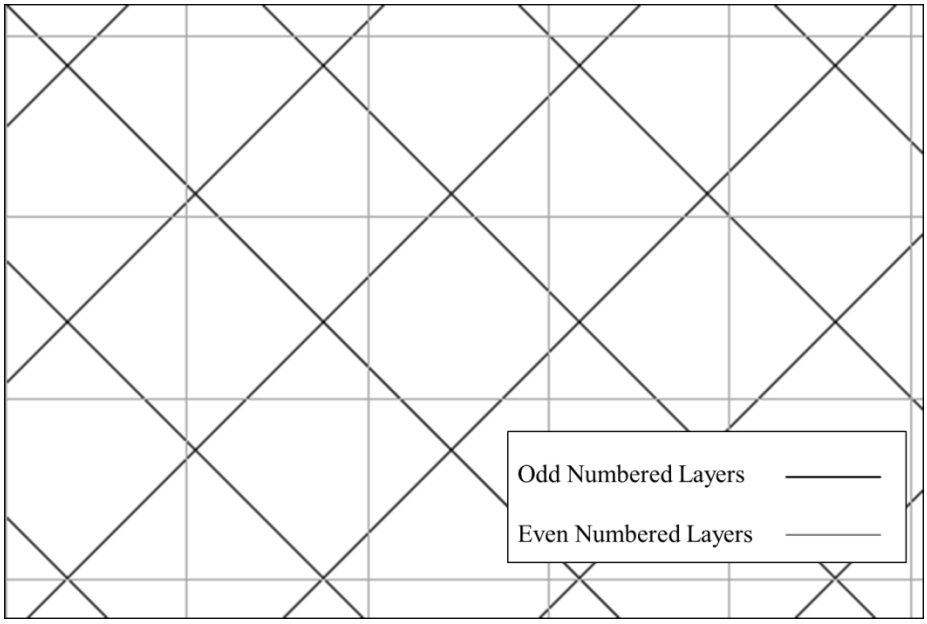


Figure 3-2: Alternating Orientation of Mesh Layer in Drop Box

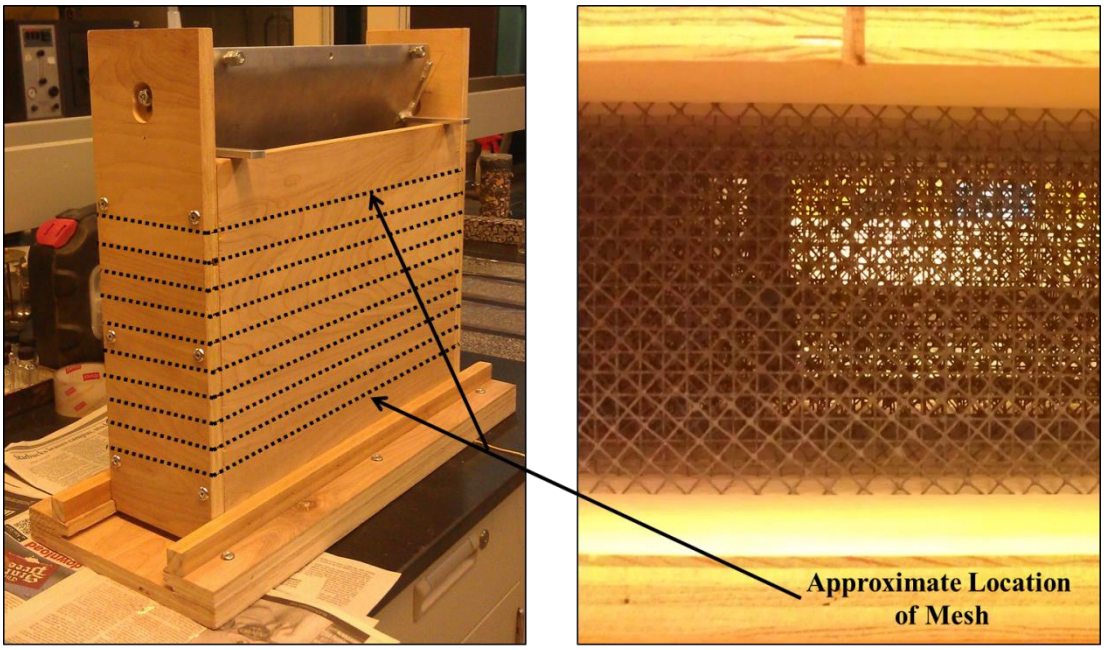

Figure 3-3: *Left* Drop Box on Base, *Right* Top View Through Mesh Layers

Dropper Mechanism

When the apparatus was being constructed, it was necessary to interpret and alter the design developed during NCHRP 4-38. The base portion of the apparatus was constructed to provide the same function as the base described from the NCHRP 4-38 report, but differed in the construction materials. The differences in the base of the apparatus are demonstrated in Figure 3-4.

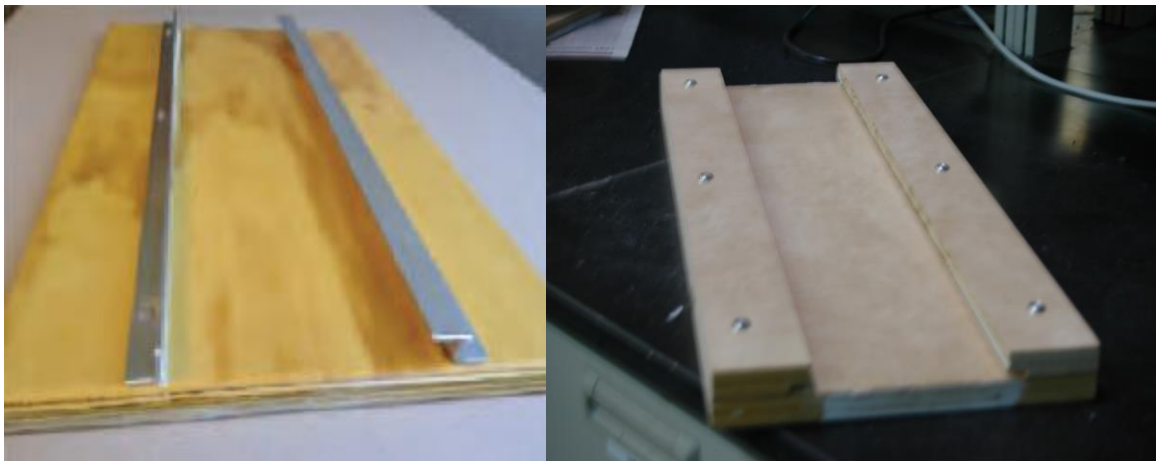

Figure 3-4: Differences Between Base of Apparatus (Right) and NCHRP Apparatus (Left)

Additionally, the NCHRP Report gave no information on the bead holder/dropper apparatus, except that it would swivel to drop the beads through the mesh box. An initial attempt to replicate this mechanism was unsuccessful and led to lateral segregation of the beads across the stripe width. Thus, it was decided that a custom bead dropper would be fabricated so that the beads could be held in place until the operator was ready to drop the beads through the box. A dropper was fabricated which opened from the bottom so that the beads would fall through the box due to gravity alone. The hopper allowed the operator to load beads into the device and spread the beads evenly along the length of the dropper. The dropper mechanism is shown in Figure 3-5.

Figure 3-5: Fabricated Bead Dropper

Drawdown Blade

An important part of the stripe fabrication process was ensuring that a consistent and repeatable film thickness could be applied to the glass plate. Part of this process involved the plywood strips that held the glass plate firmly in position. However, the major component to control the film thickness was a multi-path drawdown blade shown in Figure 3-6. This blade was purchased from The Paul N. Gardner Company, Inc. and had eight paths with gap openings of 5, 10, 15, 20, 25, 30, 40 and 50 mils. The openings in the drawdown blade did not result in an equivalent wet film thickness. As the paint dried,

it contracted so that the final dry thickness was less than the wet thickness. Combs with numerous mil openings were used to record the wet film thickness of each sample. When placed into the paint surface, some tines of the comb would touch the paint, while others would not. The actual wet film thickness was between the last tine with paint and the first tine without any paint. The wet film thickness comb is shown in Figure 3-7.

Figure 3-6: Eight Path Drawdown Blade Applicator

Figure 3-7: Wet Film Thickness Comb

*3.1.2 Initial Test Stripes*

Once the device was finalized initial test stripes were created using the sample production procedure outlined in NCHRP Report 743. The general procedure for sample preparation was as follows with a more detailed step-by-step procedure given in Appendix A:

- Weigh out the appropriate amount of glass beads
- Place beads evenly in the hopper at the top of the drop box
- Place the glass plate into the base of the apparatus
- Pour the traffic paint into a manageable container
- Place the drawdown blade on the glass plate so that the desired opening will produce the stripe
- Pour paint into the center of the drawdown blade

- Move blade lengthwise from right to left across the glass plate to produce the stripe
- Allow excess paint to fall off the glass base
- Move drop box into position on top of the base
- Drop beads through the hopper and drop box within twenty seconds of paint application

Seven sample stripes were created and the retroreflectivity was measured and recorded using a Delta LTL-X Retroreflectometer, which is shown in Figure 3-8.


Figure 3-8: Delta LTL-X Retroreflectometer

The retroreflectometer uses the emission and observation angles specified in the 30-Meter geometry and has a measurement area of 200 mm by 45 mm. The stripes were masked with duct tape so that only a central 200 mm by 45 mm area was exposed to the

retroreflectometer. For these initial trials, in addition to measuring the retroreflectivity of a central area, the retroreflectivity was measured along the stripe in order to become familiar with the apparatus, expected outcomes, and measurement area.

### *3.1.3 Image Analysis*

From these initial trials it was apparent that the number of beads on a stripe as well as their distribution, embedment, and spacing were all important factors affecting the retroreflection. It was also hypothesized that the bead distribution and nearest neighbor distance could affect the retroreflectivity through interference in the path of the light back to the device. Thus, metrics were needed in order to control the stripe-to-stripe variability (sample quality) and to index the spatial distribution and number of beads on a stripe. For this process it was necessary to count and obtain the position of the beads on the stripe. Given the sometimes large number of beads that can exist in a single stripe and the need to assign x, y coordinates to each one, it was determined that image analysis would be the most efficient and repeatable method to examine the beads and develop the necessary metrics.

In order to perform the image analysis, images of the striping samples were obtained through the use of a digital scanner. This allowed for a direct, overhead view of stripe to be obtained. Stripe samples with the airport quality beads were scanned at a resolution of 1200 pixels per inch. An example of a scanned central area image is shown in Figure 3-9.

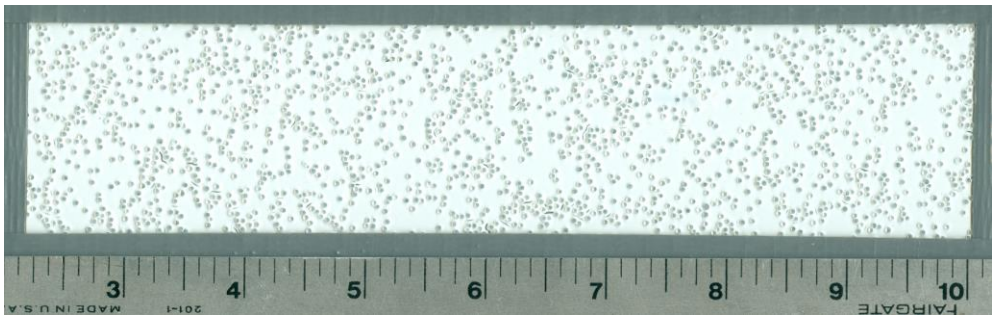

Figure 3-9: PB06 Central Area Scan

Once the scan was obtained, the image was opened in the image analysis software *ImageJ*. The software was then used to convert the image of the beads on the stripe to a binary image. Once the image was converted to a binary image, the built in analysis software was used to count and assign coordinates to the beads in the image. Counted particles were represented by an ellipse. Figure 3-10 shows part of an image where the ellipses representing counted particles are overlaid onto the original image. It can be seen that the analysis counted the darker area of the beads. This means that the data collected about each bead cannot be used for the embedment analysis, but the x, y coordinates can be used to record the position of each bead. Once the image has been analyzed, the x, y coordinates of each bead were recorded and assembled into a spreadsheet for further analysis.

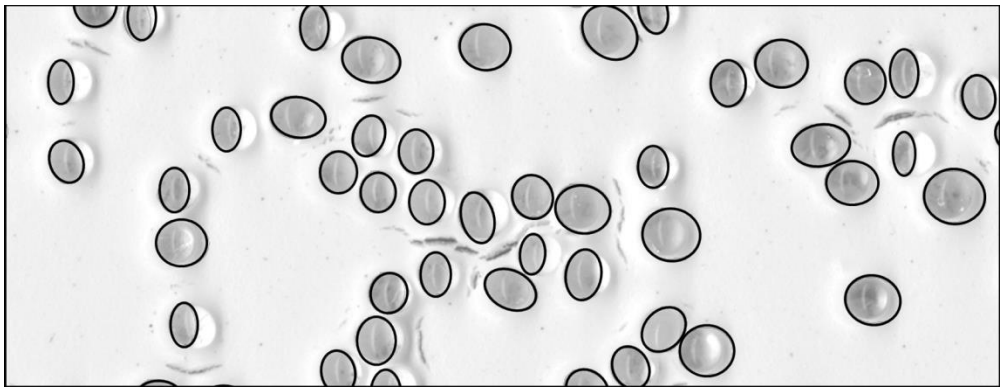
Figure 3-10: PB01 - *ImageJ* Counted Particle Ellipses Overlay on Original Image

In order to verify if the software was providing a reasonable bead count, the theoretical number of beads present in the analysis area was calculated for each application rate and bead size. The mass of beads applied to the stripe, the volume of the glass beads, and the specific gravity of glass were used to calculate the theoretical number of bead present in the measurement area. The specific gravity of glass was assumed to be 2.5. The results of this verification are shown in Figure 3-11 and

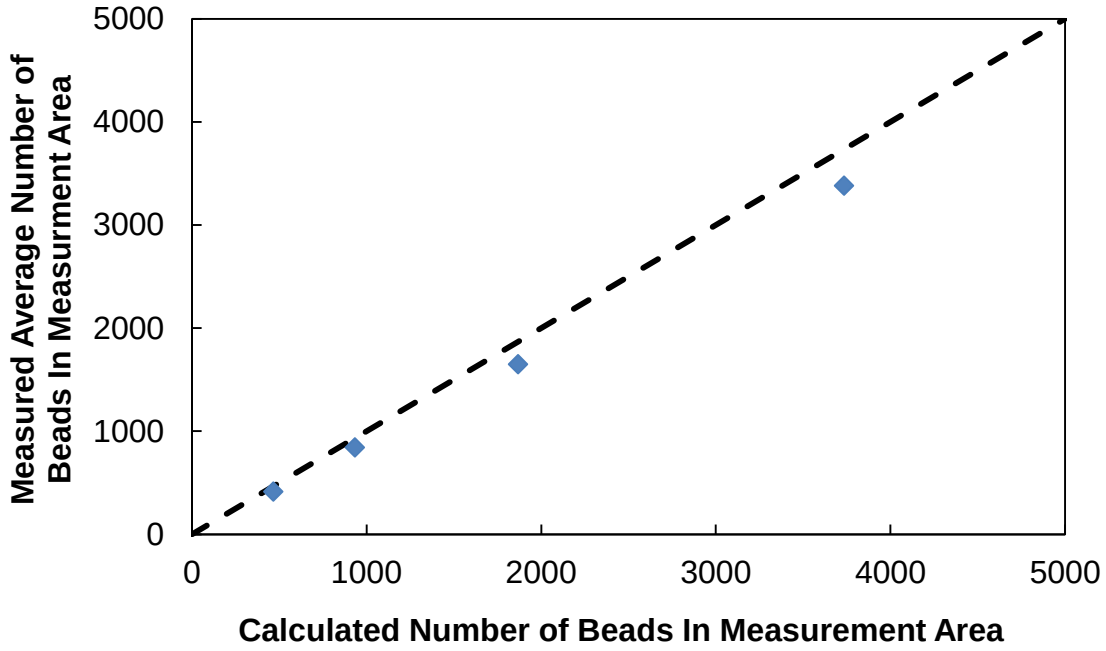


Figure 3-11: Bead Count Verification – Big Beads

The agreement between the theoretical and observed bead count is very good for the big beads. The measured bead counts are slightly below the line of equality, which implies that fewer beads are measured than expected. This is not completely unexpected, because the distribution of beads on the entire stripe is not completely uniform, which is an assumption of the calculated number of beads present.

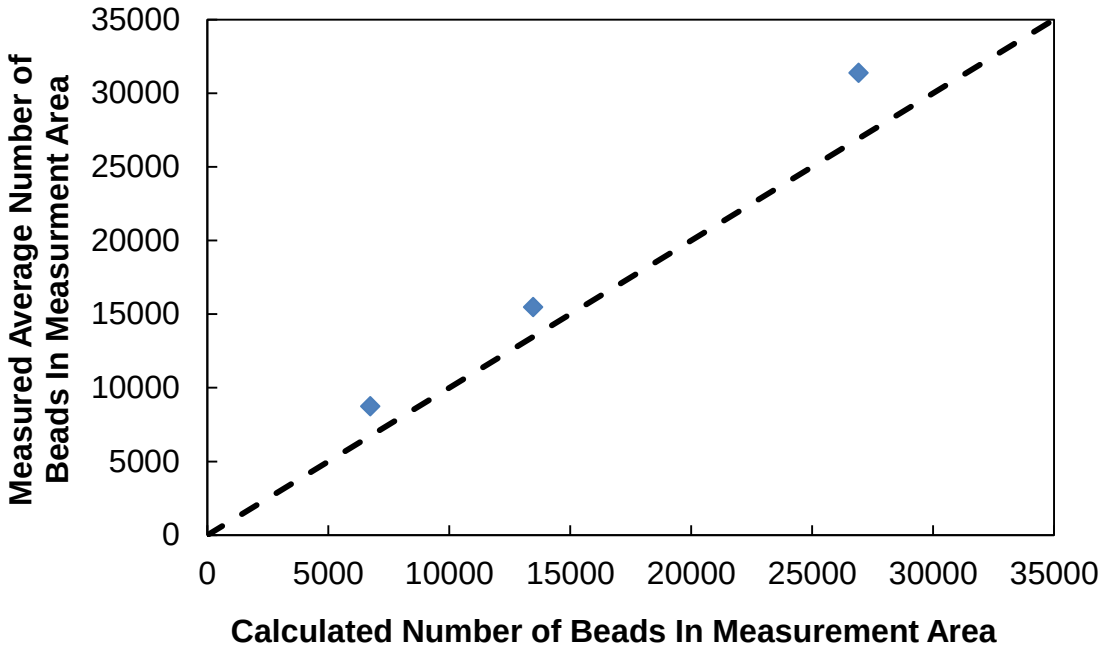


Figure 3-12: Bead Count Verification – Small Beads

Although the agreement for the small beads is not quite as good as the agreement for the big beads, it is not far from the line of equality. Once again, the calculated case assumed that the beads were evenly distributed across the entire stripe, but actual samples would not have a precisely uniform distribution of beads. Additionally, since the counting of the small beads is more difficult due to their small size and difficulty in distinguishing beads from shadows, it is more likely that some artifacts may have been counted and included in the overall analysis.

After the coordinates of the beads were recorded, the data were imported into EXCEL for further analysis. It was decided that three metrics would be used to evaluate the beads: number of beads, distance to the nearest neighbor, the Variance to Mean Ratio (VTMR), and the nearest neighbor distance in the x-direction. The number of beads counted from the image analysis served to confirm the theoretical application rate (from

mass-volume based calculations) and also to ensure that minimal loss of beads occurred within the apparatus during fabrication.

The Variance to Mean Ratio (VTMR) was used as an indicator of how well or how poorly the beads were dispersed on the stripe at a macro-level. The VTRM is used in Point – Pattern analysis as part of the Quadrant Count Method [16]. This kind of spatial analysis is sometimes used in ecological studies of plant populations. In this method, the measurement area is divided into equally sized ‘quadrants’ and the particles within each quadrant were counted. Since more than four quadrants can be used, the areas in which particles were counted will henceforth be referred to as ‘cells’. The particles in each cell were counted. Finally, the VTMR was calculated by dividing the variance between the values of the counted particles in each cell by the mean value of particles present in all cells using Equations (3.1) through (3.3).

$$s^2 = \frac{\sum \left( x - \bar{x} \right)^2}{n-1} \tag{3.1}$$

$$\bar{x} = \frac{\sum_{i=1}^{n} x_i}{n} \tag{3.2}$$

$$VTMR = \frac{s^2}{\bar{x}} \tag{3.3}$$

An example of the Quadrant Count Method using the VTMR is demonstrated in Figure 3-13, where the number of beads in each cell is shwon. The value of VTMR indicates how well dispersed the beads are on the paint stripe. It is interpreted by relating its value to the number one. Three possible outcomes exist from calculating the VTMR:

- VTMR>1: Clustered Pattern
- VTMR<1: Regularly Dispersed Pattern
- VTMR=1: Random Pattern

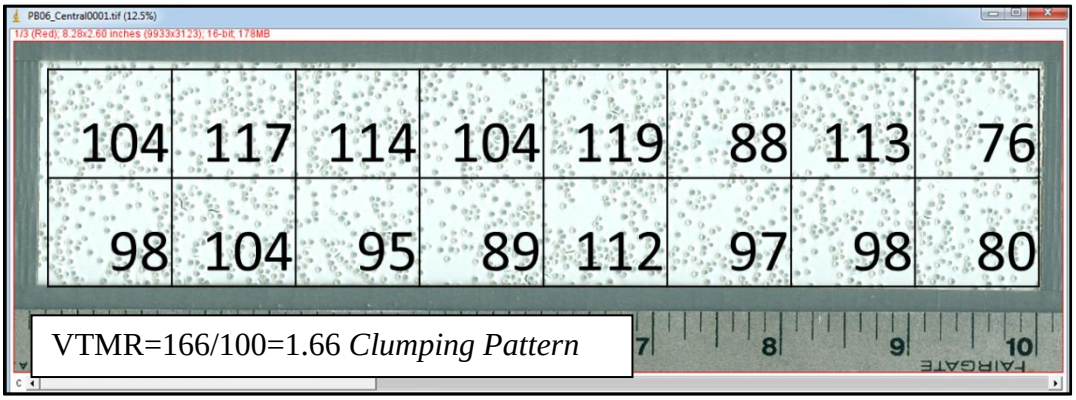


Figure 3-13: Demonstration of Quadrant Count Method

After calculating the VTMR, the nearest neighbor distance was calculated for every bead was calculated and the average value was recorded. The nearest neighbor was calculated by calculating the distance from each bead to all other beads. The minimum value was the distance to the nearest neighbor. In addition to the nearest neighbor distance, an additional distance called 'The X-Direction Nearest Neighbor' was calculated in order to see how close the beads were in the direction of lighting. This metric provides an indication of particle spacing, like the VTMR, but at a smaller scale. At the outset of this study it was unclear which scale (VTMR or X-Direction Nearest Neighbor) would control retroreflectivity and so both were evaluated.

Bead Volume Embedment Calculations Based on Spherical Geometry

The most important factor in achieving the maximum retroreflection is the embedment of the glass beads. Early on it was observed that the paint tended to form a meniscus on the sides of the glass bead due to the surface tension between the glass and the paint (see Figure 3-14 (b) versus the idealized embedment case in Figure 3-14 (a)). In this case the definition of embedment is somewhat ambiguous, and for this experiment, embedment was described based on the amount of the bead volume that was exposed. From this exposed volume, and through some geometric analysis (described below), the embedment could be calculated and is reported as the percentage of bead volume embedded. Other studies have examined the embedment of a single bead and defined embedment based on the percentage of the bead diameter exposed. These differences are recognized and have been taken into account in the analysis presented in this thesis.

To measure the embedment of the beads on the stripe two different methods were adopted. For stripes with beads embedded at 50% or more, the overhead scanned image was used, whereas stripes from beads with less than 50% embedment a side view based camera technique was developed. For beads that were embedded greater than 50%, it is clear that their apparent diameter would be smaller than the true bead diameter. Figure 3-14 demonstrates the difference between the bead diameter and the exposed diameter due to the paint film thickness. As the thickness of the paint increases, the exposed diameter of the bead decreases. By assuming that the beads are spherical a measurement of the exposed diameter of a bead allows the embedment depth to be calculated. Once the embedment depth is calculated, the amount of the bead embedded in the paint can be

calculated as a percentage of the total bead volume. This process is facilitated by using the geometry of a partial sphere as shown in Figure 3-14 (d).

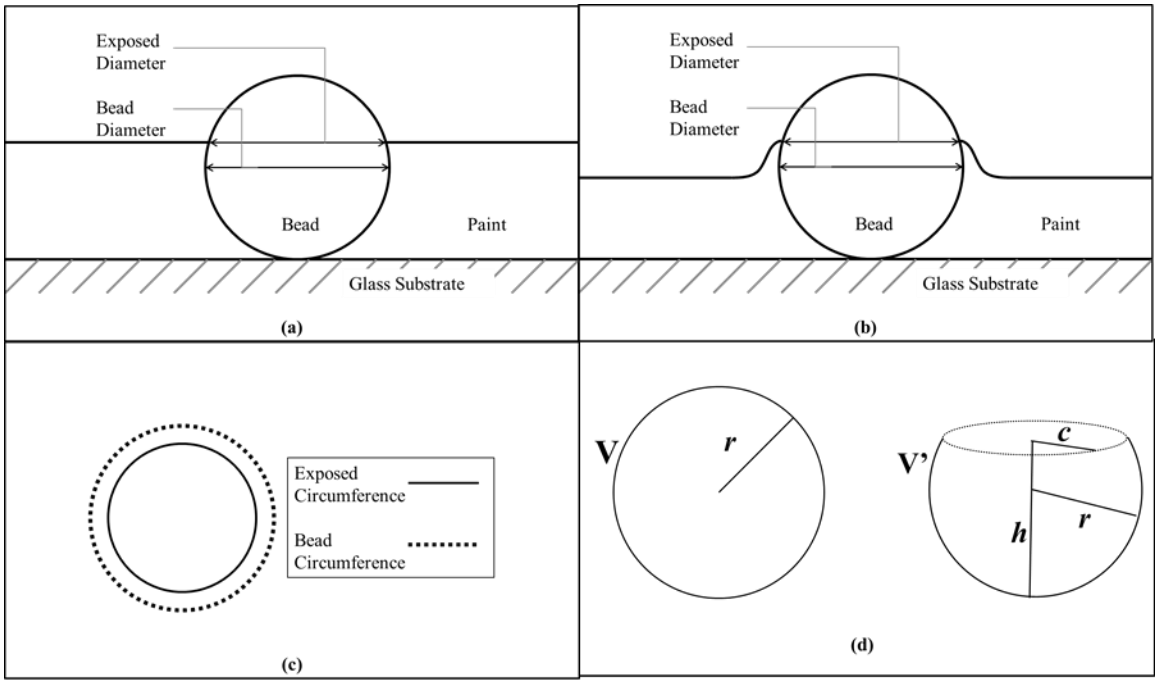


Figure 3-14: (a) Side View of Embedded Bead – Idealized, (b) Side View of embedded Bead – Actual, (c) Top View of Embedded Bead, (d) Volume Parameters of a Sphere and Partial Sphere

For samples where beads are embedded greater than fifty percent, the top- view digital scan was used to measure the exposed bead diameter. The process began by opening the image in *ImageJ* and setting the appropriate scale. In a separate spreadsheet, thirty random x, y coordinate pairs were generated. Next, the image was examined in order to locate beads at the randomly generated x, y coordinates. If a bead was not present at any set of coordinates, the nearest bead was selected for measurement. To calculate the exposed diameter of a bead at the given coordinates, a line was drawn in *ImageJ* in both the x and y orientations. The exposed diameter was then calculated be averaging the exposed diameters measured in the x and y directions. Once the measurements were completed on all thirty points, the overall average exposed diameter was calculated.

To calculate the percentage of bead embedment, three values were required: absolute bead diameter ($r$), exposed bead diameter ($c$), and height depth of embedment ($h$). From the previous step, the exposed radius was calculated by dividing the exposed diameter by two. For this process the actual diameter of the beads should be known. The beads in all trials were carefully sieved to provide as near to uniform sized beads as possible. In addition, calibration samples were prepared wherein the bead diameters were measured using the same image analysis software used to find the exposed diameter of the beads. This analysis was conducted separately from the stripe samples and confirmed that the beads chosen had a uniform diameter with 84% of the diameters falling within 7% of the mean value. By measuring $c$ and assuming the average radius $r$, the height $h$ was calculated using Equation (3.4). Equation (3.5) was used to calculate the volume of the spherical bead embedded in the paint. Finally, the percentage of the bead volume embedded in paint was calculated by comparing the embedded volume to the overall volume of the bead. The overall volume of a bead was calculated using Equation (3.6).

$$c = \sqrt{h(2r - h)} \tag{3.4}$$

$$V' = \frac{\pi}{6} h\sqrt{3c^2 + h^2} \tag{3.5}$$

$$V = \frac{3}{4}\pi r^3 \tag{3.6}$$

For beads which were embedded less than fifty percent, an alternate calculation needed to be conducted. It would be impossible to see the exposed diameter of a bead which was embedded less than fifty percent from a top-down view because the beads

were not transparent enough to see the exposed diameter. Therefore, in order to calculate the percentage of bead embedment, angled photos were taken and analyzed.

For side-view imaging the stripe sample was placed at an angle of 14.63° and the camera was placed in front of the sample as level as possible. Marks were placed on the sample in order to divide the sample in thirds. When taking images of the sample, it was not possible to have the whole third of the sample in focus. So the focus length was adjusted so that a band of beads would be in focus in the image. Two images of each third were obtained so that two bands of in-focus beads could be analyzed.

As with the overhead method, thirty points were randomly selected for embedment analysis. Since two images were obtained for each third of the sample, six images in total would be used to calculate the embedment of the beads on the stripe. Five beads from each sample were analyzed. Figure 3-15 demonstrates the in-focus areas in each third of a sample. From each image, five beads were examined and the percentage of embedment was calculated using the overall bead radius and the exposed height.

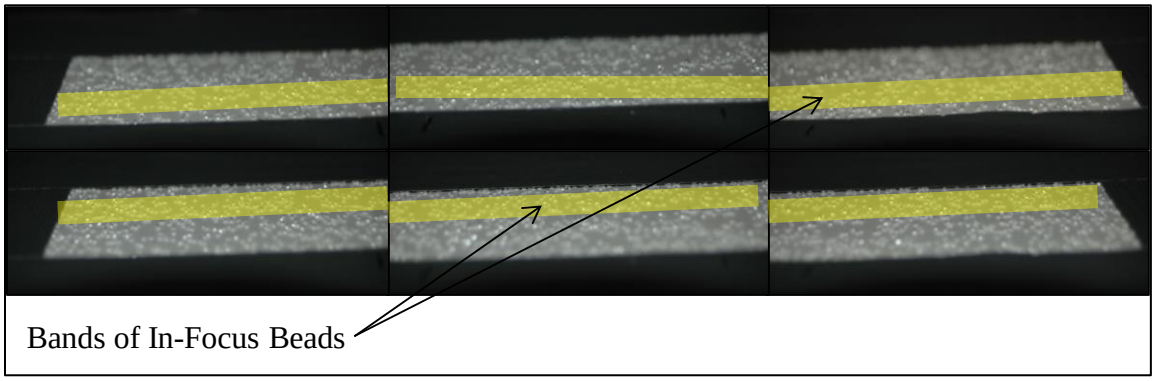


Figure 3-15: Bands of In-Focus Beads in Side View Embedment Calculation

Using Equation (3.4), the observed bead radius and bead height were measured and the variable *c* was calculated for each bead observed. As with the greater then 50% embedded cases, the volume of the partial sphere embedded and exposed were calculated.

It should be noted that since the images were taken at an angle and not from a directly horizontal side view, the measured height needed to be corrected a more accurate bead height could be used to calculate the exposed volume. A drawing a bead at an angle of 14.63° and a correction value was calculated and applied to the recorded height measurements.

### *3.1.4 Novel Contributions to Apparatus and NCHRP Procedure*

The apparatus described in Section 3.1.1 was constructed using specifications outlined in NCHRP Project 4-38. Although the description of the apparatus was sufficient to construct the apparatus, specifics on how to build the apparatus were lacking. Some liberties were taken in the construction of the apparatus which included the mesh screen orientations and the bead dropper mechanism. Specifically, the bead dropper mechanism was constructed so that the beads would drop straight down through the mesh box without any rolling movement. Once loaded into the dropper, the bottom of the dropper opened up beneath the beads when the operator was prepared to drop the meads through the mesh screens. The mesh layers were installed in alternating ninety and forty-five degree orientations, which were not specified in the apparatus specifications. Construction of the apparatus was simple and was constructed with readily available materials.

The most significant alteration to the procedure outlined in NCHRP Project4-38 was the addition of image analysis to better estimate the embedment of the glass beads. The procedure outlined in the report relied on a visual verification to check if the beads were embedded approximately 60%. Although the percent of bead volume embedment could be estimated from the wet film thickness measurement, there are other factors

which contribute to the overall embedment of the beads. For example, as the application rate increases, the amount of paint displaced by the beads also increases. As a result the paint creeps further up the sides of the beads increasing the overall bead embedment. The meniscus of the paint creeps up the sides of the bead (as shown in Figure 3-14b) resulting in deeper embedment. By using image analysis, the average percent embedment of the beads can be better estimated by observing the actual exposed diameter of embedded beads. By measuring the exposed diameter and using spherical geometry, the meniscus effects of the paint can be taken into account. Figure 3-16 shows that using image analysis can resulted in a percent embedment value which can differ from the percent embedment calculated from the film thickness. It can also be seen that the small beads show a greater amount of embedment than the film thickness suggests. This is because the large amount of beads results in a greater surface area for meniscus effects to alter the embedment when compared to the small beads. Image analysis also provides a more objective evaluation of the bead embedment than examining the embedment visually by eye.

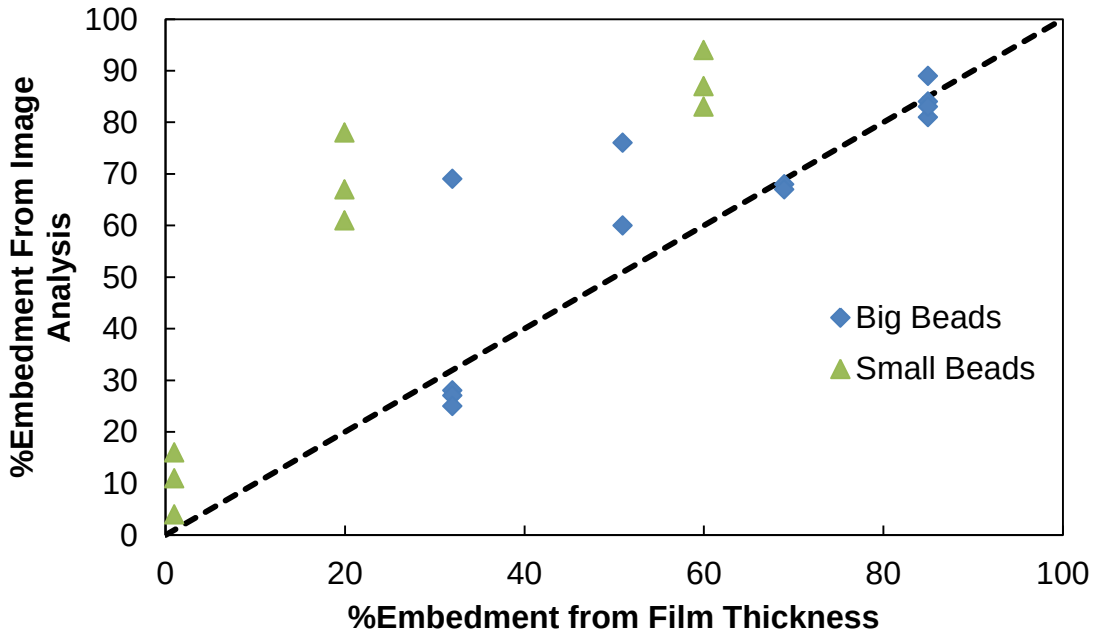


Figure 3-16: Percent Embedment Calculated From Film Thickness and Image Analysis

### 3.2 Phase II: Production of Samples with Airport Quality Beads

Phase II consisted of incorporating the lessons learned from Phase I and creating samples for analysis. A uniform gradation of -16+20 mesh glass beads was used. This translates to possible bead diameters ranging from 1.19mm to 0.841mm. A sample of beads was placed on the scanner and analyzed in order to measure the average diameter. For big beads the average diameter was found to be 1.01mm. Based on the definitions given earlier, these are considered to be 'large beads' and would be used in *airport quality* glass bead mixes. It was decided to use uniformly sized large beads in order to ensure that the procedure used to create the striping samples could be altered in such a way as to vary the embedment of the beads at the various application rates. Four application rates were used in order to observe the effect of various application rates on the retroreflectivity of the stripes.

### *3.2.1 Sample Preparation*

The goal of Phase II was to use the procedure from Phase I to observe the relationship between embedment percentage and retroreflectivity for different bead application rates. It was decided early-on that the materials evaluated in this project should reasonably reflect in-service materials. From a review of the literature including the Arizona Department of Transportation's specifications [4],[18][19] it was found that a nominal rate of 6 lb/gal (6 lb of beads per gallon of paint) was typical. Thus, this rate was chosen as the basis for further experiments. These units, while very useful in field applications, resulted in some issues for this laboratory study. Recall that the primary purpose of this project was to evaluate the individual and combined effects from embedment depth and particle spacing. Thus it was necessary to control one or the other variables and adjust the other, e.g., maintain the bead density but vary the embedment depth. Since it was difficult to directly control the embedment (embedment occurred due to gravity) the decision was made to control embedment by reducing the thickness of the paint. However, reducing the thickness of the paint effectively increased the dosage rate of the beads since less paint was applied to the stripe. Here, the dosage rate (6 lb/gal) is used as a surrogate measure for bead density (beads/mm$^2$) and is accurate only at a wet film thickness of 15 mil. This approach was taken as a means to interpret the data efficiently, but also as a way to generalize the findings for application to thermoplastics where the stripe thickness may be many times the diameter of the bead and embedment depth can be more carefully controlled by adjustments to the thermoplastic temperature. The amount of beads applied to each sample was recorded as the mass of beads applied to the stripe. The mass of the beads applied was kept constant for each application rate, thus

using the around the same number of beads on each sample while changing the paint film thickness. For example, it was found that 13g of big glass beads would equal the 6lb/gal bead application rate. The 13g was kept constant over multiple samples and classified as 6lb/gal, even though the true application rate changed as the paint thickness changed.

In addition to the 6 lb/gal rate, it was decided to make samples which would represent a 3 lb/gal, 1.5 lb/gal, and 12 lb/gal rate in order to observe the change in retroreflectivity with the number of beads on the stripe. Recall, for this thesis the application rate, although presented as a lb/gal rate, was really a bead mass per stripe rate. Although the area of retroreflectivity measurement is only 200 mm x 45 mm as stated in Section 3.1.2, the size of the whole stripe on which the bead were dropped was 4″ x 18″. The mass of beads applied to the stripe for each application rate are presented in Table 3.1.

Table 3.1: Application Rate Defined as Bead Mass Per Stripe

| **Bead Mass/Stripe (grams)** | **Application Rate (lb/gal)** |
|---|---|
| 3.25 | 1.5 |
| 6.5 | 3 |
| 13 | 6 |
| 26 | 12 |

The testing of lower application rates would simulate the loss of beads over time while the testing at higher application rates would evaluate the potential impacts from over application of the beads. The initial experimental matrix involved creating five samples at the 6 lb/gal rate in order to characterize the general behavior of the retroreflectivity versus embedment curve. Once the general trend was seen, three samples would be produced at the other rates. As it will be discussed in Section 4.3, the original

matrix was expanded upon as gaps in the data were observed and as the feasibility creating samples at all the embedment values was evaluated. The initial Phase II production matrix is show in Table 3.2.

Table 3.2: Phase II Production Matrix

| | | % Embedment | | | | |
|---|---|---|---|---|---|---|
| | | **40** | **50** | **60** | **70** | **80** |
| **Big Beads** | **6lb/gal** | | | | | |
| | **6lb/gal rep** | | | | | |
| | **3lb/gal** | | | | | |
| | **1.5lb/gal** | | | | | |
| | **12lb/gal** | | | | | |

### 3.3 Phase III: Production of Samples with Road Quality Beads

Phase III incorporated the lessons from both Phases I and II in order to produce and analyze samples made with *road quality* beads. A uniform gradation of -40+50 mesh glass beads was used. This translates to possible bead diameters ranging from 0.420mm to 0.297mm. A sample of beads was placed on the scanner and analyzed in order to measure the average diameter. For big beads the average diameter was found to be 0.415mmThe size of these beads classified them as a component of road quality beads. It was decided to use only three application rates; 6lb/gal, 3 lb/gal, and 1.5 lb/gal. This was decided after observing how many beads were retained on the paint surface and observing that the 12 lb/gal rate would result in a large number of beads that could not be embedded. Additionally, since the road quality beads were much smaller than the airport quality beads, the thickness of the paint was limited to 5 mils and 10 mils with the apparatus from Phases I and II. Paint was then also applied at a 1 mil thickness through

the use of a custom made drawdown blade shown in Figure 3-17. The same sample production procedure from Phases I and II was used in Phase III.

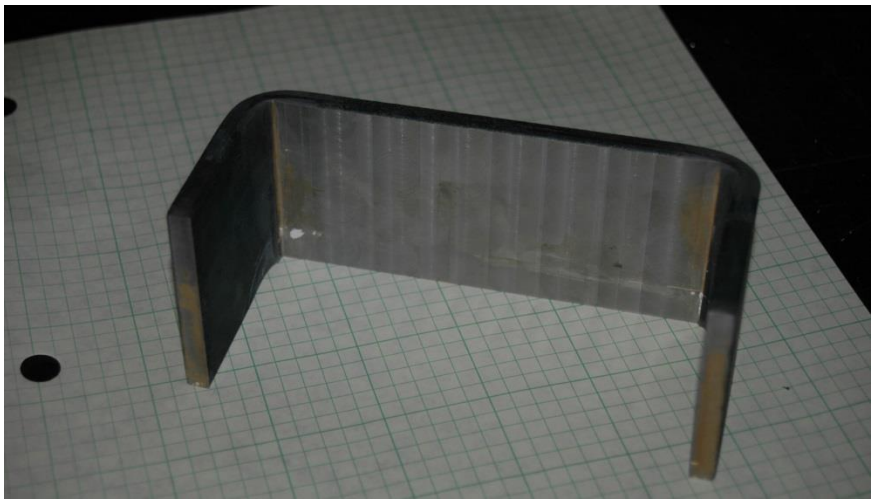

Figure 3-17: Custom 1 Mil Opening Drawdown Blade

# Chapter 4 Effect of Striping Parameters on Retroreflectivity

## 4.1 Introduction

The results of the three phases of experimentation are discussed in this chapter. From these results, the percent embedment at which the retroreflection was maximized was shown to agree with literature. The overall maximum application rate for large beads was estimated. Using the results from the large bead samples, a model was developed to predict retroreflectivity given the number of beads, nearest neighbor in the x-direction, and the distribution of bead embedments. The following sections show and discuss the various results from each phase of experimentation.

## 4.2 Preproduction Samples

One of the primary goals for Phase I of this research study was to build familiarity with the fabrication and testing procedures. For this purpose, a few stripes were manufactured and tested once the apparatus was fully developed and the analysis metrics drafted. Since these stripes were important for establishing the experience needed to meet the primary objective of this research, but were not directly used to in the data collection that addressed that objective they have been referred to as the pre-production samples. After these pre-production samples were made, the retroreflectometer was used to measure the retroreflectivity of each. The results of the pre-production samples are presented in Table 4.1.

Table 4.1: Assembled Data of Preproduction Samples

| Stripe | Bead Count | Bead Mass (g) | VTMR | Retroreflectivity | Embedment (% volume) | Production Order |
|---|---|---|---|---|---|---|
| L-1 | 1765 | 17 | 4.35 | 561 | 62.6 | 1 |
| L-2 | 2226 | 17 | 3.79 | 531 | 83.6 | 2 |
| L-3 | 2941 | 23 | 0.93 | 532 | 80.9 | 3 |
| L-4 | 1372 | 11 | 1.89 | 499 | 84.7 | 5 |
| L-5 | 864 | 5.2 | 2.1 | 451 | 66.4 | 6 |
| L-6 | 1732 | 17 | 0.84 | 630 | 58.3 | 7 |
| S-1 | NR | 23 | NR | 89 | NR | 4 |

Preproduction Sample04 represented a quick experimentation with small beads. The analysis metrics had not yet been developed for the small beads, thus the retroreflectivity is the only recorded metric for Sample 04. All other samples were produced with the large beads at varying application rates and embedment depths. The samples were produced in this way to observe the change in the retroreflectivity readings while learning how to operate the retroreflectometer. A graphical representation of the results from the preproduction samples is presented in Figure 4-1. Note that these samples represent both changing application rates and changing percent embedment. For example, between sample L-1 and L-2 the retroreflectivity decreased as the percent embedment increased from sixty to eighty percent. Samples L-1, L-2 and L-6 were made with the same application rate. L-6 achieved the highest retroreflection and was closest to the optimal embedment of 60 percent. Additionally, the lower VTMR of L-6 may also explain why it attained a higher retroreflectivity than L-1. Throughout the preproduction samples, different levels were achieved, which gave confidence that the procedure could be used for the rest of the experimentation. Overall, as familiarity with the apparatus improved (e.g., as more samples were made) the VTMR decreased.

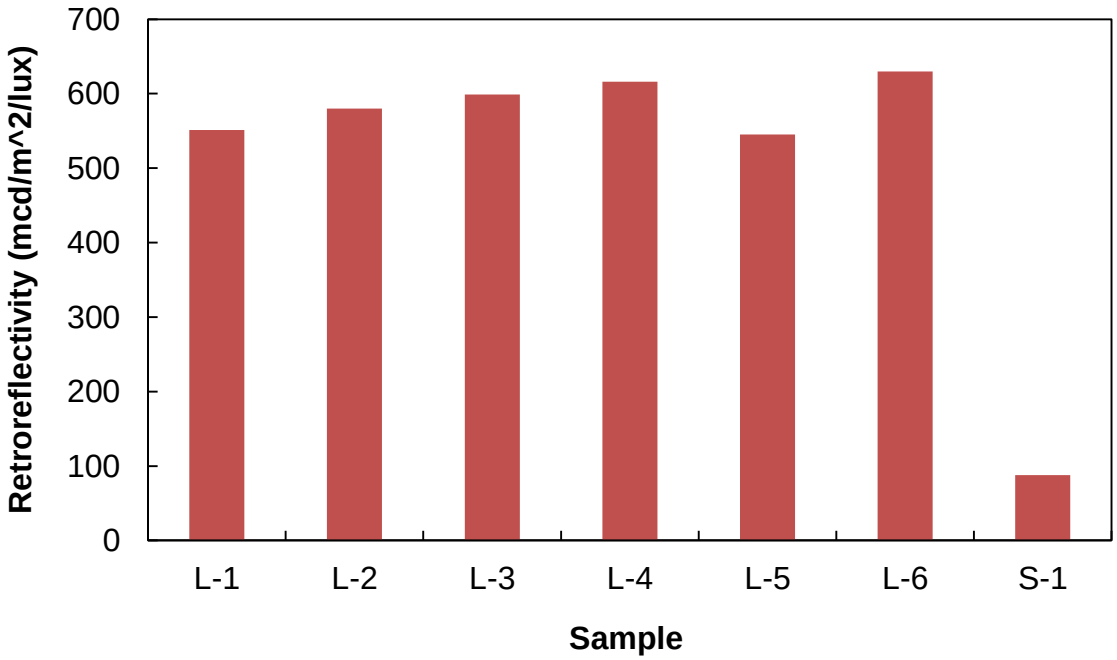


Figure 4-1: Retroreflectivity of Preproduction Samples

In addition to obtaining the retroreflectivity in the center of the stripe, the first four preproduction samples were used to observe the evolution of retroreflectivity along the stripe length. This was accomplished by positioning the center of retroreflectometer at the edge of the beaded area of the stripe. Retroreflection readings were then taken along the stripe by repositioning the retroreflectometer in one inch increments along the stripe length. Each reading represented a different position along the stripe and captured the effect of varying the number of beads exposed to the retroreflectometer as well as the variation in retroreflectometer readings. This evolution of retroreflection is shown in Figure 4-2. In each case, the retroreflectometer began to capture the drop in retroreflection at the ends of the stripe. This occurred because the measurement window began to include edge areas where no beads had been applied. The results from this

examination of retroreflectivity gave confidence that the measurements in the middle of the stripe would be representative of the stripe as a whole.

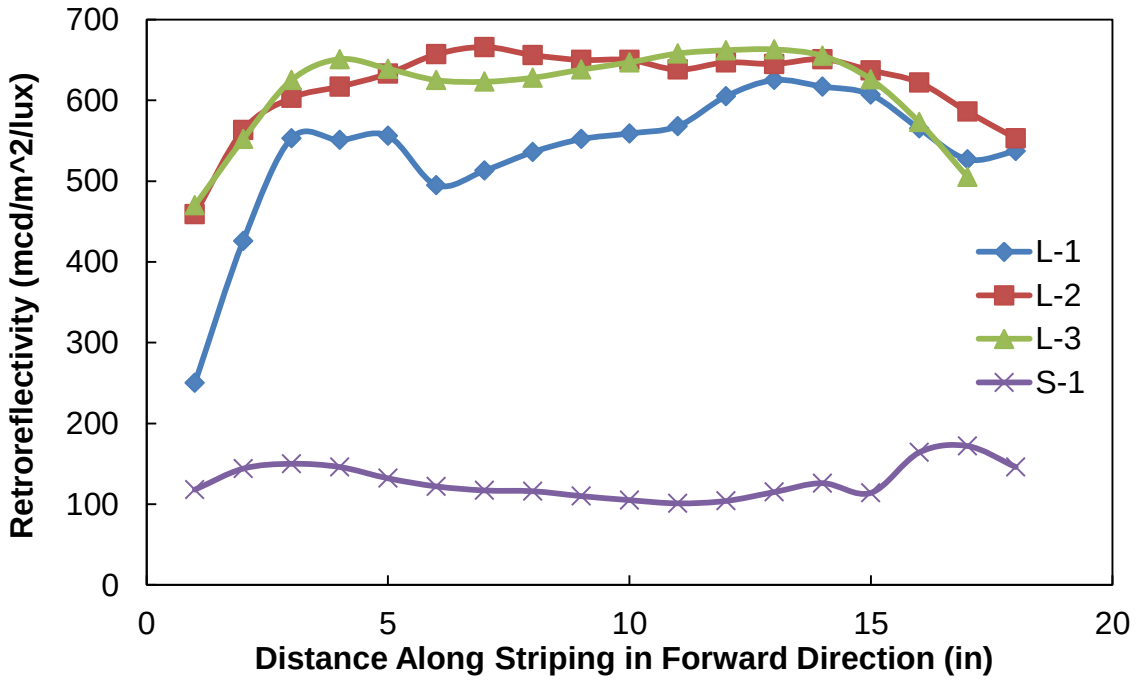

Figure 4-2: Evolution of Retroreflectivity Along Four Preproduction Samples

From Figure 4-2 it can be seen that variability exists throughout the length of the stripe. The standard deviations in retroreflectivity for these samples are shown in Table 4.2. It can be seen from the standard deviation values that L-1 was the most variable of the four samples presented. Since sample L-1 was the first sample produced, it is expected that it would have the highest variability. Throughout the four preproduction samples, the variability decreased dramatically in the center eight inches of the stripe, which is also the area in which the retroreflectometer operates.

Table 4.2: Retroreflectivity Standard Deviation of Four Preproduction Samples

| | **L-1** | **L-2** | **L-3** | **S-1** |
|---|---|---|---|---|
| Std. Dev. (18” length) | 85.42 | 51.31 | 56.34 | 21.09 |
| Std. Dev. (Center 8”) | 45.47 | 7.98 | 16.22 | 8.49 |

## 4.3 Large Bead Production Samples

The goal of Phase II was to evaluate the relationship between the percentage of bead volume embedment and retroreflection and its interaction with bead application rate. To meet this goal, stripe samples were created with varying bead application rates and paint thicknesses. In addition, the application rate which would produce the maximum retroreflection value was calculated from the results. The various analysis metrics were examined in order to see if any additional correlations to retroreflection could be observed.

As samples were produced and the percent embedment was evaluated, the original production matrix was expanded upon as shown in Table 4.3. Due to the limited sized openings in the draw down blade, it was not feasible to produce samples at forty percent embedment for all application rates. For instance, a 3 lb/gal sample was twenty percent embedded at a 5 mil drawdown blade opening, but sixty percent embedded at a 10 mil opening. Additionally, when beads were dropped onto the paint, the higher application rates deposited more beads and displace more paint than the samples produced at the lower application rates.

Table 4.3: Big Bead Adjusted Production Matrix

| Production Matrix | | | | | | | |
|---|---|---|---|---|---|---|---|
| | | % Embedment | | | | | |
| | | 20 | 40 | 50 | 60 | 70 | 80 |
| Big Beads | 6lb/gal | | PB04 | PB01 | PB03 | | PB05 |
| | 6lb/gal rep | | | | PB02 | | PB06 |
| | 3lb/gal | PB13 | | | PB07, PB16 | | PB08 |
| | 1.5lb/gal | PB14 | | | | PB09 | PB10 |
| | 12lb/gal | Pb15,PB17 | | | PB18 | PB12 | PB11 |

The LTL-X retroreflectometer was used to measure the retroreflectivity of each of the samples shown in Table 4.4. The percent embedment was calculated for each sample using the procedures outlined in Section 3.1.3. The retroreflection versus embedment percentage plot is shown in Figure 4-3.

Table 4.4: Big Bead Retroreflectivity vs. Percent Embedment Results

| Sample | Application Rate (lb/gal) | Percent Embedment (%volume) | Retroreflectivity (mcd/lx/m$^2$) |
|---|---|---|---|
| PB09 | 1.5 | 73.91 | 293 |
| PB10 | 1.5 | 85.85 | 249 |
| PB14 | 1.5 | 27.06 | 87 |
| PB07 | 3 | 67.60 | 601 |
| PB08 | 3 | 81.41 | 457 |
| PB13 | 3 | 25.26 | 160 |
| PB16 | 3 | 61.20 | 420 |
| PB01 | 6 | 36.66 | 442 |
| PB02 | 6 | 67.98 | 508 |
| PB03 | 6 | 68.73 | 609 |
| PB04 | 6 | 34.12 | 375 |
| PB05 | 6 | 84.04 | 519 |
| PB06 | 6 | 83.80 | 549 |
| PB11 | 12 | 83.47 | 450 |
| PB12 | 12 | 76.18 | 330 |
| PB15 | 12 | 28.00 | 178 |
| PB17 | 12 | 29.88 | 194 |
| PB18 | 12 | 68.78 | 378 |

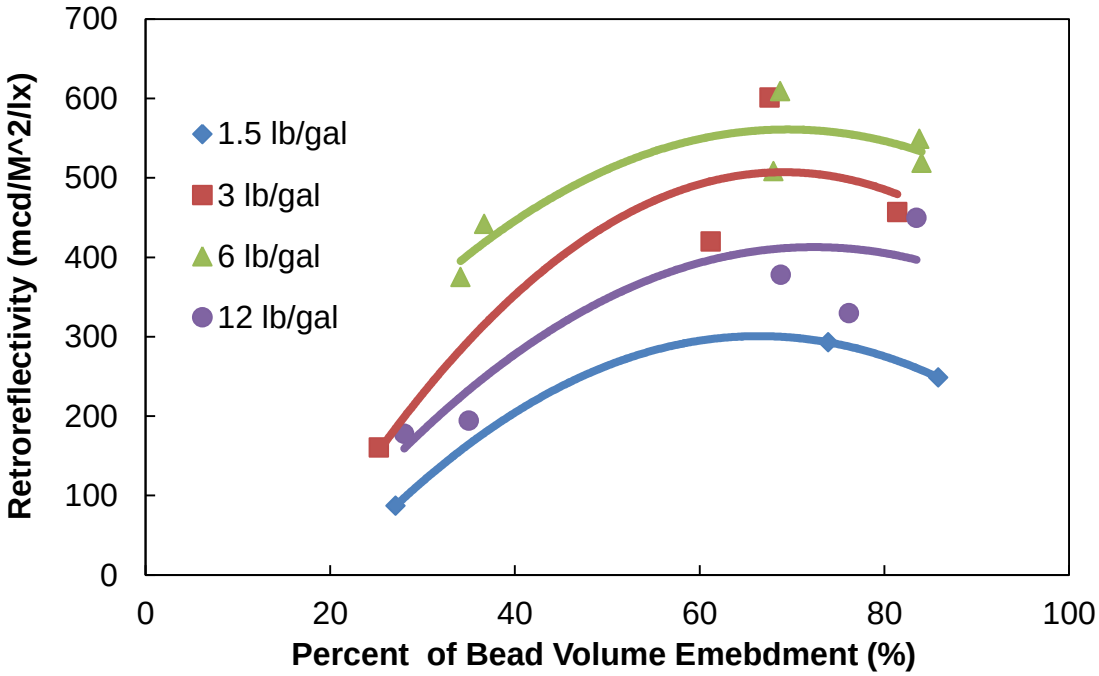

Figure 4-3: Retroreflection vs. Percent Embedment Phase II

It can be seen from Figure 4-3 that bead application rate can have a profound impact on the stripe retroreflectivity. As the application rate increased from 1.5 lb/gal to 6 lb/gal, the retroreflection also increased. Additionally, the data shows that doubling the application rate from 1.5 lb/gal to 3 lb/gal raises the retroreflectivity substantially. A similar doubling of the rate from 3 lb/gal to 6 lb/gal results in an increase of the retroreflectivity, but not by the same amount as the 1.5 lb/gal to 3 lb/gal increase. Interestingly, the change in rate from 6 lb/gal to 12 lb/gal results in a decrease in retroreflection. One theory that may explain why the drop in retroreflection occurs between the 6 lb/gal and 12 lb/gal cases is that when too many beads are present on the stripe surface light interference between the beads occurs, which bends the light away from the usable retroreflection angles. In addition to the blockage of light entering the

bead, bead interactions could also interfere with light exiting from nearby beads. The 30-meter geometry illustrated in Figure 2-2 shows that the difference in the incidence and observation angle is only 1.05 degrees. If the beads are too close together in the direction of the incidence, then a bead may block the light which would have entered the bead close to it as shown in Figure 4-4.

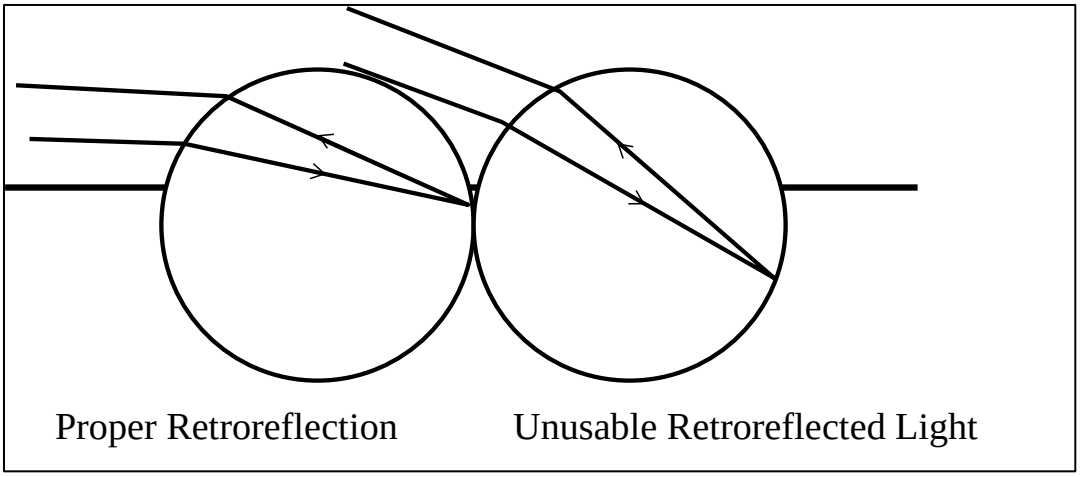


Figure 4-4: Bead Interaction Blocks Usable Light

The trendlines for each application rate shown in Figure 4-3: Retroreflection vs. Percent Embedment Phase II were drawn with second order polynomial equations. The equations, $R^2$ values, and embedment values which result maxima for each trendline are presented in Table 4.5. Note that only three data points exist in the 1.5 lb/gal rate; thus, the $R^2$ value of this data set equals one because a second order polynomial only requires three points in order to be defined. It can be observed from Table 4.5 that the coefficients for the 12 lb/gal, 6 lb/gal, and 1.5 lb/gal rates are similar except for the y-intercept value. The y-intercept value is responsible for shifting the trendline vertically, so it is expected that the y-intercept between two trendlines would be different.

Table 4.5: Phase II Trendline Data

| **Application Rate (lb/gal)** | **Trendline Equation** | **Embedment Which Results in Maximum (% Volume)** | **$R^2$** |
|---|---|---|---|
| 1.5 | $Y=-0.14x^2+18.33x-307.91$ | 66.4 | 1.00 |
| 3 | $Y=-0.22x^2+29.87x-463.18$ | 66.8 | 0.92 |
| 6 | $Y=-0.13x^2+18.38x-77.73$ | 68.9 | 0.81 |
| 12 | $Y=-0.13x^2+18.64x-261.71$ | 70.1 | 0.76 |

In order to determine the optimal application rate, the trendline equations were used to develop the relationship between the number of beads on the stripe and the retroreflection. The bead count was calculated by taking the average of all the bead counts in each application rate. The result of this comparison is shown in Figure 4-5. Each curve in Figure 4-5 represents a different percentage embedment. Each application rate is represented a constant average bead count throughout each percent embedment series. It can be seen that for the all application rates, that the maximum retroreflection value occurred at approximately a 68 percent embedment (66.4% – 70.1%), which is slightly higher than that predicted by the single bead studies of Grosges [1]. Additionally, it can be seen that a bead count approximately equal to 2,000 would result in the greatest retroreflection across all embedment percentages. A bead count of 2,000 translates to a bead application rate of approximately 7 lb/gal, which is within the typical range as discussed in Section 3.2.

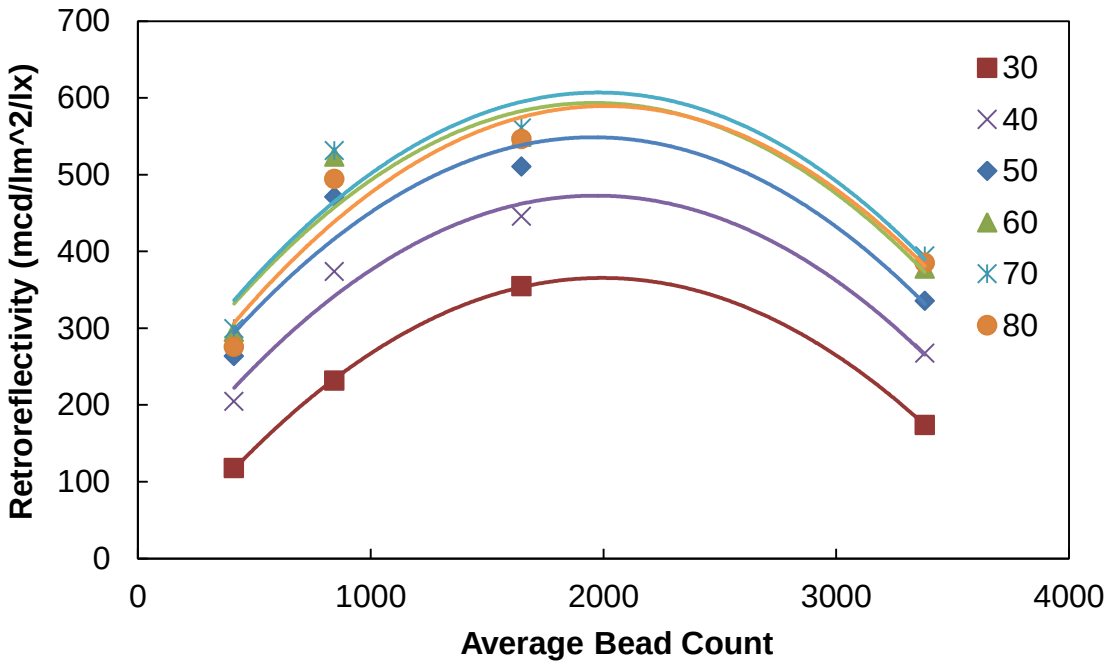

Figure 4-5: Average Bead Count versus Retroreflection at Various Percent Embedment

The various analysis metrics were examined to see if any correlation to the retroreflectivity could be observed. Although the amount of retroreflection is primarily affected by the percent embedment, special parameters could explain any observed drop in retroreflection due to bead interference. The nearest neighbor distance for each sample was calculated by calculating the nearest neighbor distance for each bead and taking the average of all beads. The nearest neighbor distances vs. retroreflectivity for the big bead samples are shown in Figure 4-6.

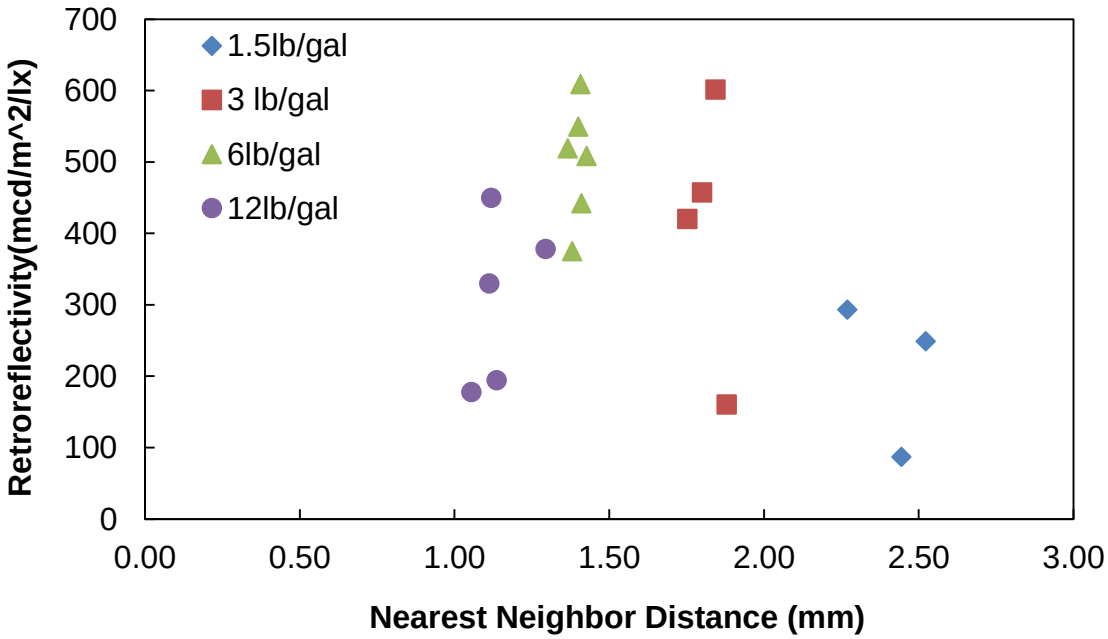


Figure 4-6: Nearest Neighbor Distance vs. Retroreflection Phase II

It can be seen that each application rate is primarily associated with a specific range of nearest neighbor distances. It is difficult to observe a trend since the retroreflectivity can change dramatically between the samples as the embedment changes, but the neighbor distance remains fairly constant. However, where retroreflectivity values are similar, the sample with a slightly greater nearest neighbor distance has the higher retroreflection. Additionally, the effect of nearest neighbor distance may play a greater role when there is more potential for interference. The nearest neighbor distance in the 12 lb/gal case is very close to the overall bead diameter of 1.01mm, which suggests that beads are almost to the point of touching and that the distance between them approaches the length of one bead diameter on average.

## 4.4 Small Bead Production Samples

Following the same procedures from Phase II, samples were made including road quality beads. For the small bead samples, the paint was sourced from a different manufacturer, but was still white, latex, traffic paint. The diameter of the small beads was 0.415 mm on average, about 40% smaller than the big beads. Because of this difference, the 5 mil and 10 mil openings on the drawdown produced samples with a much greater percent embedment. A custom drawdown blade, shown in Figure 3-17, was constructed to obtain an embedment less than 50 percent. As samples were produced, it was noted that not all the beads applied at the 6 lb/gal rate were adhering to the stripe. This suggested that the 12 lb/gal application rate would not be obtainable with the small beads, thus 6lb/gal, 3 lb/gal, and 1.5 lb/gal application rates were used for the samples in Phase III. The retroreflection versus embedment data is shown in Table 4.6, and demonstrated graphically in Figure 4-7.

Table 4.6: Small Bead Retroreflectivity vs. Percent Embedment Results

| Sample | Application Rate (lb/gal) | Percent Embedment (%volume) | Retroreflectivity (mcd/lx/m$^2$) |
|---|---|---|---|
| PS03 | 1.5 | 67 | 325 |
| PS06 | 1.5 | 93.53 | 449 |
| PS09 | 1.5 | 11.54 | 136 |
| PS02 | 3 | 71.88 | 346 |
| PS05 | 3 | 87.93 | 453 |
| PS08 | 3 | 15.89 | 98 |
| PS01 | 6 | 78.37 | 212 |
| PS04 | 6 | 83.43 | 360 |
| PS07 | 6 | 3.93 | 154 |

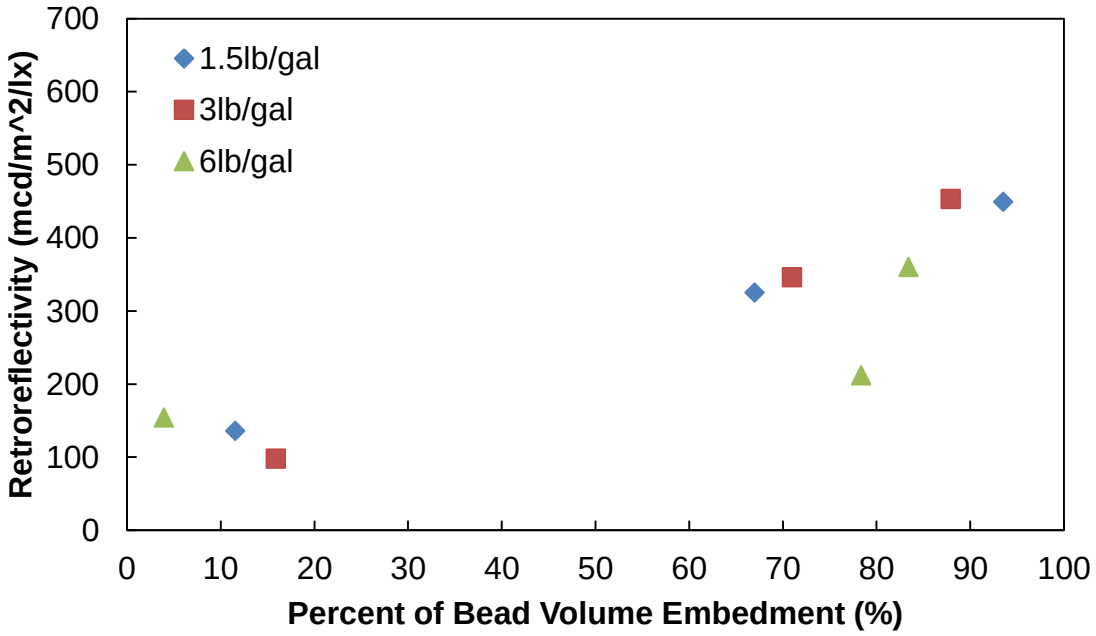


Figure 4-7: Retroreflection vs. Percent Embedment Phase III

It can be seen from Figure 4-7 that the samples with small beads did not show the same trend as the big bead. It is thought that the high percent embedment and variability of the retroreflectometer measurements combined result in data that do not capture the theoretical maximum retroreflection between sixty and seventy percent embedment.

Form the small bead results, a similar trend can be observed in relation to the application rate. In this case, the 6 lb/gal application rate showed a decrease in retroreflection. Although the 6lb/gal rate is within the normal range of application rates, and although the beads used in this phase are road quality beads, the small beads are at the upper limit of road quality beads. In a typical bead mix, only a small portion of the beads would be as large as these beads. Since the beads are the largest component of a normal bead mixture, it makes sense that using the typical application with these beads may also result in similar interference observed with the 12lb/gal case with the big beads.

## 4.5 Development and Verification of Initial Retroreflectivity Model

When examining the results presented in Figure 4-3, it can be seen that when one compares the results from this experimentation to the retroreflection versus embedment curve shown by Grosges in Figure 2-6, the experimental results demonstrate that retroreflection is retained as the samples deviate away from the sixty percent optimum. The Grosges figure suggests that the intensity of retroreflection at the optimal embedment is much greater than the intensity at other embedment depths.

Assuming that the phenomenon Grosges presents exists for one bead, it was decided to use the idea of a band of retroreflected intensity to model the retroreflection of the bead samples. It was decided that Grosges' intensity curve could be modeled as a Gaussian function as shown in Figure 4-8. This function acts as an intensity kernel which is applied to each bead sample. The parameters of the Gaussian equation are the mean value, standard deviation, and a multiplier factor.

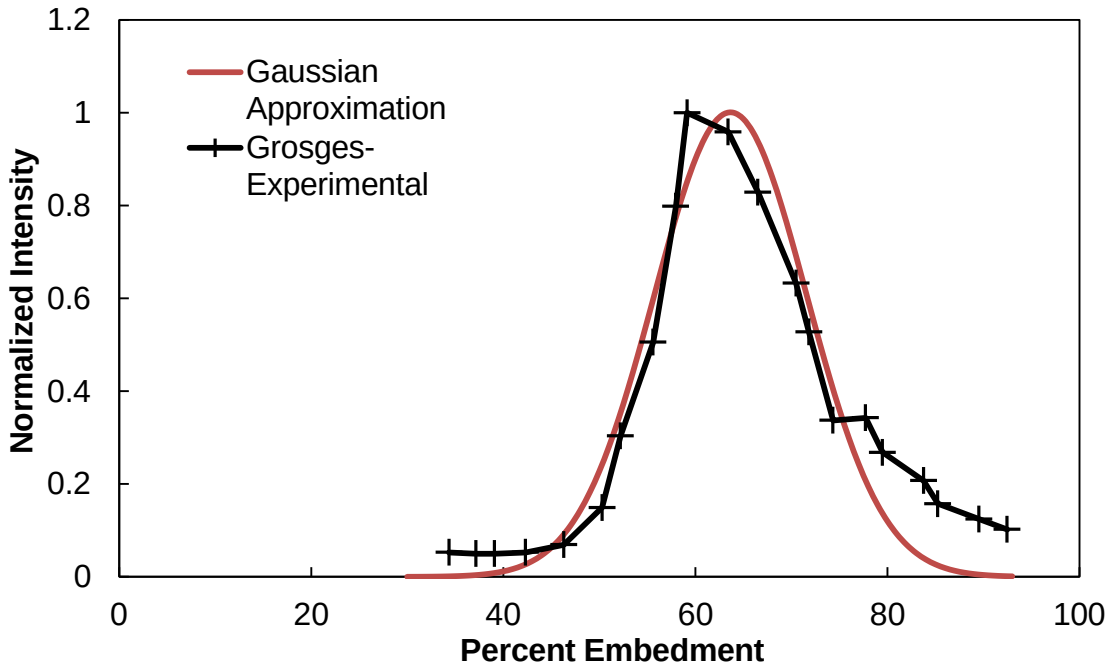

Figure 4-8: Gaussian Interpretation of Grosges Intensity Kernel

Beginning with the 1.5 lb/gal cases, the parameters of the intensity kernel were optimized so that the kernel would closely predict the retroreflectivity of the 1.5 lb/gal cases. . The 1.5 lb/gal case was chosen because the beads are far enough apart that light interference is less likely to occur. Instead of using the average percent embedment, the percent embedment was calculated for all thirty bead examined in the image analysis. From the embedments, a histogram was constructed showing the frequency of beads with particular embedments. The histogram was developed for Bin values from ten to one hundred percent embedment with an increment of three. From the thirty frequencies, the number of beads at each percentage embedment was calculated incorporating the total number of beads on the sample. Then number of beads at each embedment depth was then multiplied by the intensity value at the same embedment depth. From this, the intensity of retroreflected light was calculated for the number of beads at each percent embedment.

The addition of all intensities for the various embedments resulted equaled the retroreflectivity. The intensity kernel was then optimized using Solver to accurately predict the retroreflectivity of the 1.5 lb/gal case.

Once the intensity kernel was optimized for the 1.5 lb/gal case, the kernel was applied to the 3 lb/gal, and 6 lb/gal cases. For the 12 lb/gal case, the measured retroreflectivity was lower than the 6 lb/gal case. However, the model would have resulted retroreflectivity values higher than the 6 lb/gal cases. As discussed earlier in this section, the proximity of the beads to each other causes light interference and therefore decreased the retroreflectivity in the 12lb/gal cases. It was determined that a spacing factor should be applied to the model so that the effect of light interference could be incorporated. The X-Direction Nearest Neighbor distance was used as the basis for the spacing factor. The spacing factor itself was modeled as a sigmoidal function, which resulted in a factor of 1 for the majority of 1.5 and 3 lb/gal cases and a value of approximately 0.2 for the 12lb/gal cases. The shifting function is shown in Figure 4-9.

After incorporating this shifting function, the model was used to predict the retroreflectivity of all big bead samples. The measured and predicted values were plotted against the line of equality. The result of the model prediction is shown in Figure 4-10.

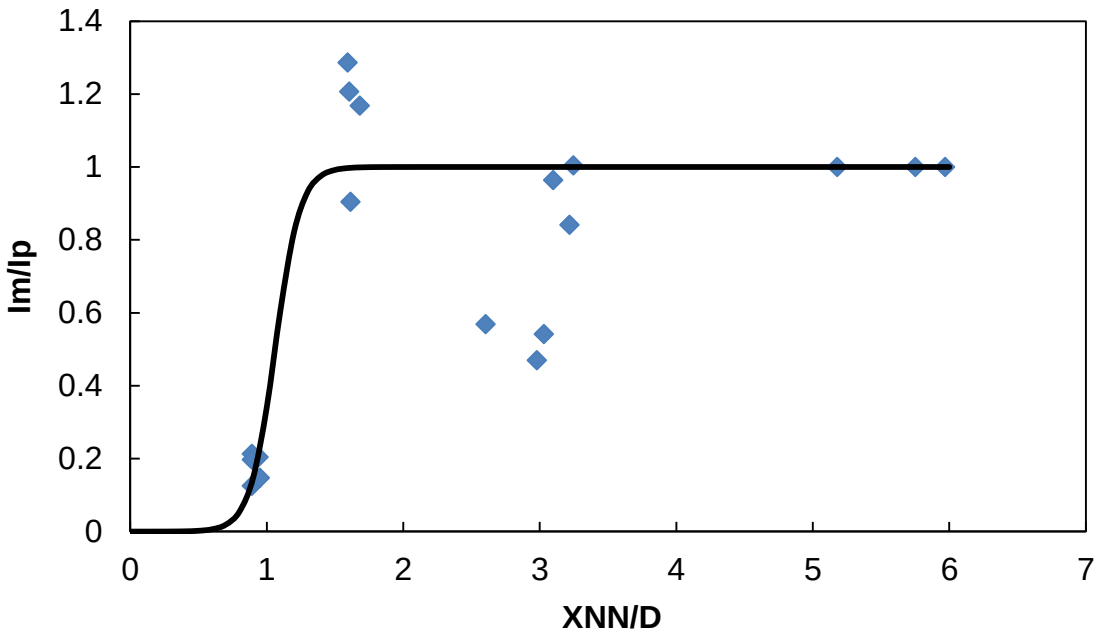


Figure 4-9: Sigmoidal Shifting Factor Function for Phase II Samples

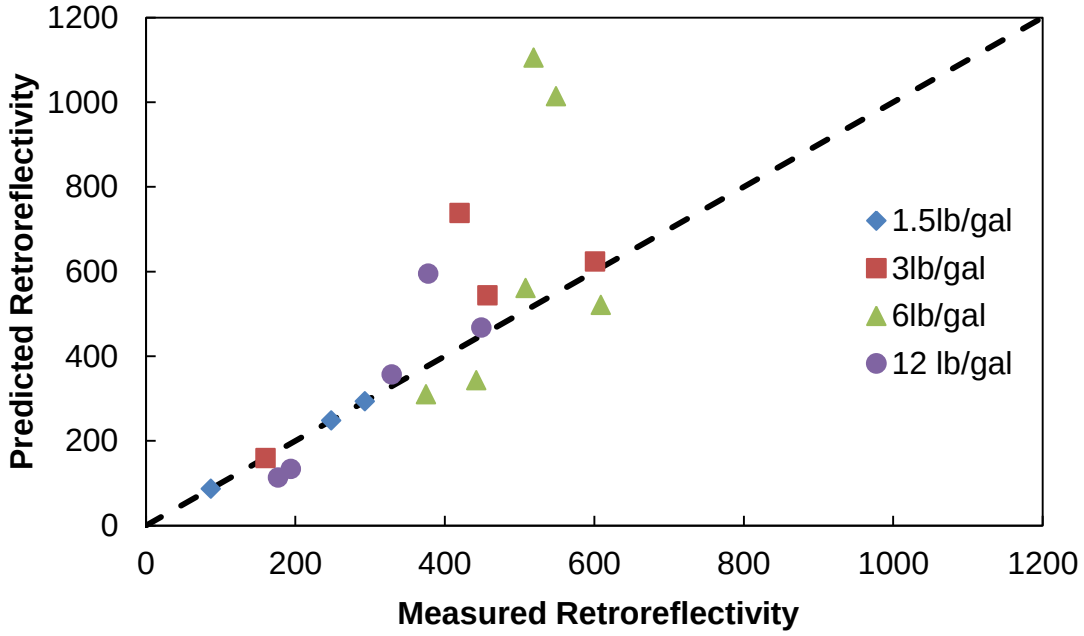


Figure 4-10: Predicted vs. Measured Retroreflectivity

It can be seen from Figure 4-10, that the model would provide a fair prediction for the majority of cases. Note that since the model was built from the 1.5lb/gal cases, the points

which belong to the 1.5 lb/gal dataset are almost directly on the line of equality. The shifting factor was also able to predict the retroreflectivity values for the 12lb/gal case. Recall that the 12lb/gal case resulted in a lower retroreflectivity than the 6lb/gal case. The model was able to reflect this drop due to the addition of the shifting factor. Although two points in the 6 lb/gal case are quite over-predicted by the model, the three of the remaining four points straddle the line of equality.

After the model was developed for the big beads, the same kernel was applied to the small beads. The mean and standard deviation of the intensity kernel were kept the same, but the intensity value was optimized for the small beads. It was assumed that the small beads would be capture less light because the surface area is smaller than the surface area of the big beads. The small beads were then used to test the model. The model was set to recreate the small bead samples. The measured and predicted retroreflectivity were recorded. The results of testing the model with the small bead samples are shown in Figure 4-11.

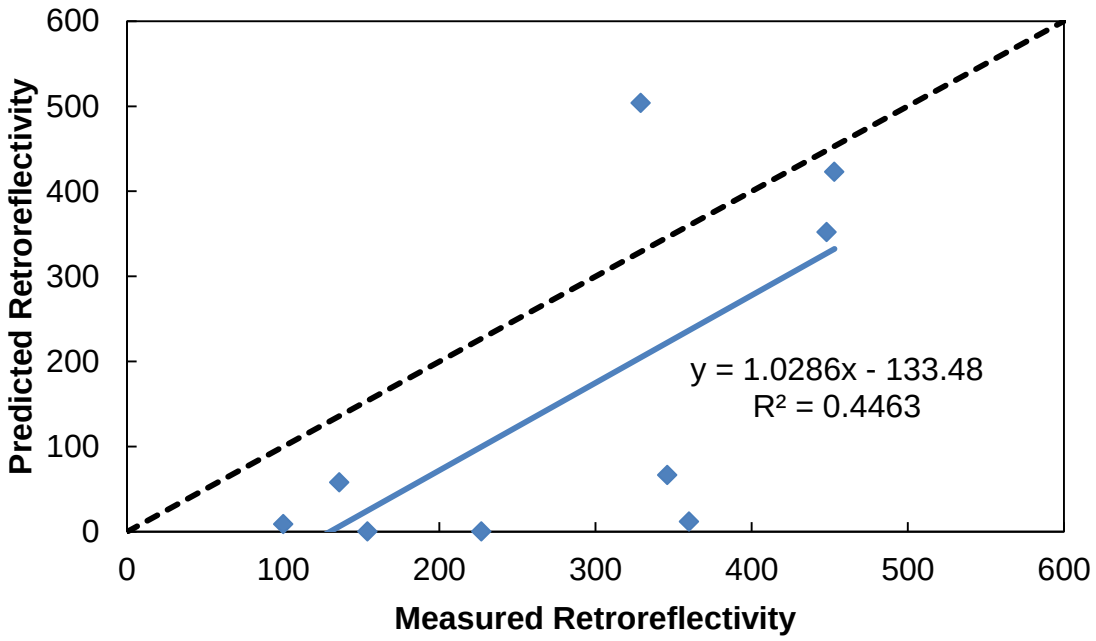


Figure 4-11: Testing Model with Small Bead Samples

From the result of testing the model with the small beads it can be seen that the slope of the best fit line is almost equal to one. The vertical offset from the line of equality demonstrates that the model does not capture a factor in the small bead retroreflectivity. One reason the model may under predict the retroreflectivity of the small is that the meniscus effects would be magnified in the small bead samples when compared to the large bead samples. Additionally shifting factor from the big beads may not be applicable to the small beads, because the intensity kernel did not represent the small beads as well as the big beads. Figure 4-10 showed that in general, the intensity kernel was a fair approximation of the big bead samples, but this was not the case for the small beads.

### 4.6 Parametric Evaluation

Even though the data from the small bead samples could not verify the model, the model was used to produce artificially generated retroreflectivity versus embedment curves. The outcome of generating the retroreflection curves is shown in Figure 4-12.

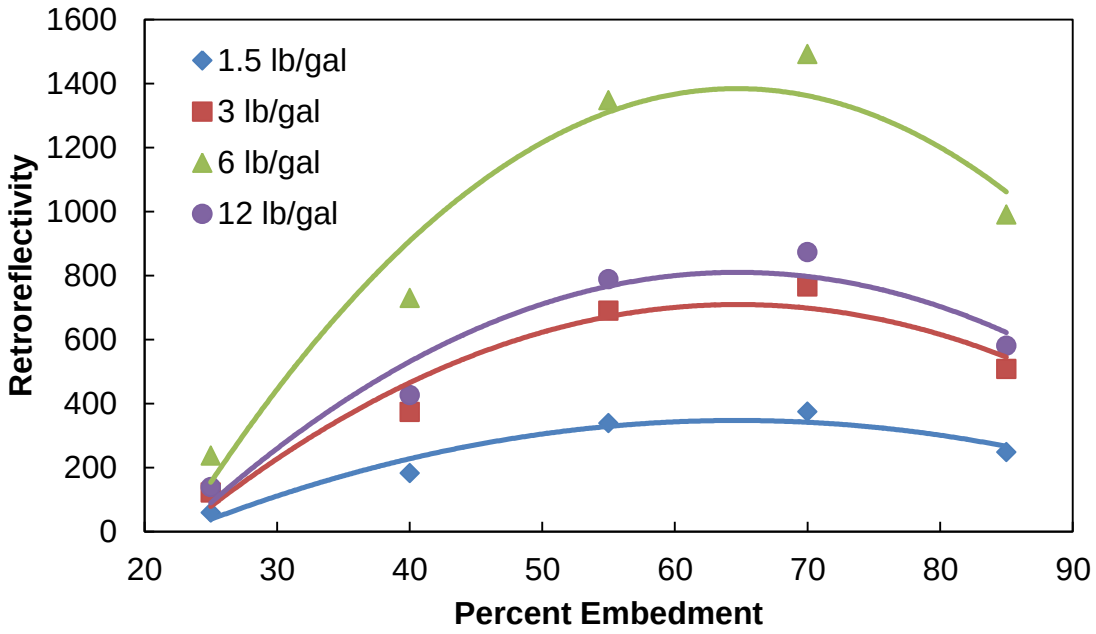


Figure 4-12: Artificially Generated Retroreflectivity vs. Embedment Curves

Figure 4-12 was then compared to the retroreflectivity vs. embedment curves from the big bead samples shown in Figure 4-13.

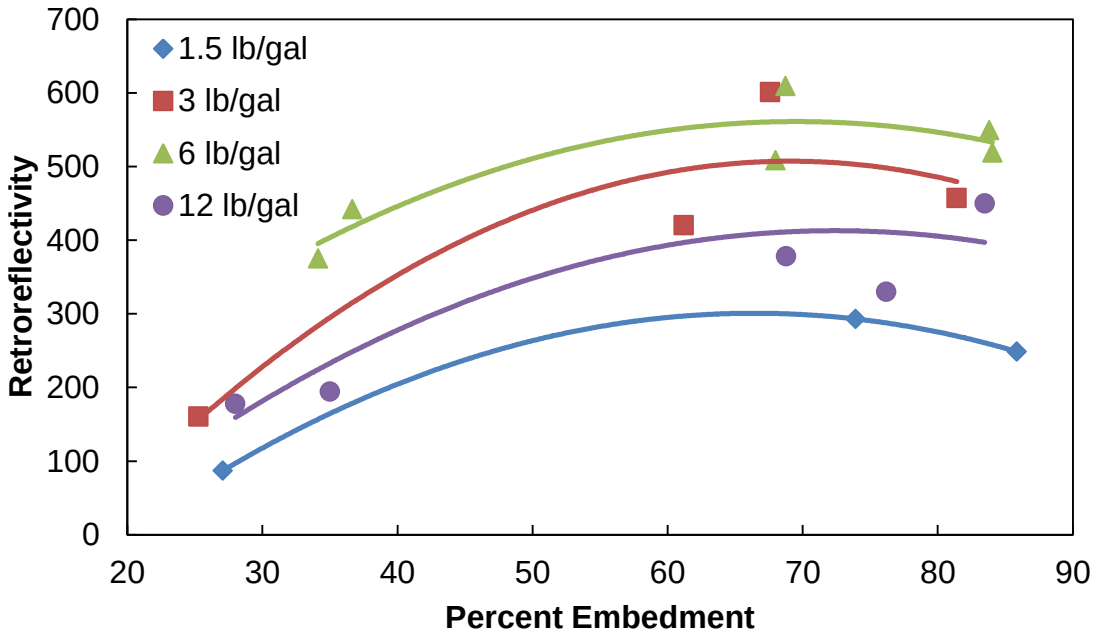


Figure 4-13: Embedment vs. Retroreflectivity Phase II Results

When one compares Figure 4-12 and Figure 4-13, it can be seen that the 6lb/gal rate is considerably more arched and has a higher retroreflection in general when compared to the original data. A reason for this may be that, in general, the 6lb/gal rates considerably more over predicted by applying the intensity kernel when compared to the other rates (Figure 4-10). Additionally, the simulated 12lb/gal rate has a greater retroreflection than the 3lb/gal rate, while the opposite is shown by the real data. Although the trendlines of the simulated data follow a broad curve, the data points themselves more closely resemble the Gaussian shape of Grosges' intensity curve. This is expected since the data suggested a broad curve and the model uses a narrower Gaussian intensity Kernel. Finally, the trendlines of the generated retroreflectivity curves suggest that across all application rates, the maximum retroreflection is achieved when the beads are embedded around sixty-five percent, which is consistent with both the literature and with the results from Phase II.

The overall model can be described in the following form:

$$R = S(Xnn / D)\sum_{0}^{100} I(E_i) * N(E_i) \qquad (4.1)$$

$$I(E_i) = \frac{1}{2\pi} e^{-\frac{(E_i - B)^2}{2C^2}} * A \qquad (4.2)$$

$$N(E_i) = \frac{f(E_i)}{\sum_{i=10}^{i=100} f(E_i)} * BeadCount \qquad (4.3)$$

$$S(XNN / D) = \frac{H}{1 + e^{(-F*(\frac{XNN}{D} - G)}} \qquad (4.4)$$

Where *R* is the total retroreflection intensity, *XNN* is the X Direction Nearest Neighbor distance, *D* is the bead diameter, *BeadCount* is the number of beads present on the sample, $E_i$ is the particular percent embedment i, $f(E_i)$ is the number of beads at embedment percentage $E_i$, and A, *B*, *C*, *F*, *G*, *H* are constants obtained from the optimization with big beads.

Due to limited time and resources, additional refinement to this model was not possible. It is suggested that additional striping sample be made and analyzed. The model should then be re-optimized to account for the additional data. Additionally, although other analysis metrics were considered for the shifting function, a better fit may be accomplished by using some combination of spatial factors to define the shifting function.

## Chapter 5 Conclusion and Future Work

From experimentation with large beads, the theoretical optimal percent embedment was found to be between sixty-five and seventy percent. This agrees with various sources which claimed an optimal retroreflection near sixty percent embedment. The results from Phase II and Phase III also suggest that there are an optimal number of beads which contribute to retroreflection. As the number of beads on the stripe increases, the retroreflection increases up to a point after which the bead density became so great that the bead geometry results in light interference. Although the light may still enter the bead, the angle at which it is retroreflected is of use to a vehicle operator. Using data from Phase II, the maximum application rate of large beads was calculated to be approximately 7 lb/gal, which is within the typical range of bead application rates.

Using data from Phase II, a model was developed to estimate the retroreflectivity of a stripe given the X Direction Nearest Neighbor distance, bead size, application rate, bead count, and distribution of bead embedment percentages. The data was used to artificially generate retroreflection vs. embedment curves which exhibited a similar behavior to the large bead samples. Although the 6 lb/gal application rate is particularly over estimated, the same general trends can be observed between the big bead data and the generated data. Alterations and verification of this model with the small beads is left for further work.

Image analysis allowed the percent embedment of particular beads to be calculated. For the various analyses, the average bead diameter was used. Future refinements in the image analysis could allow much more data to be collected about the striping samples in a more automated fashion. If image analysis could be used to estimate

the exposed diameter for every bead, then the percent embedment of each bead could be calculated. Refinements and increased automation of the image analysis procedure would allow for a quicker analysis of the striping samples.

In order to create striping samples, the apparatus was constructed using specifications outlined in NCHRP Project 4-38. Although the description of the apparatus was sufficient for construction, specifics on how to build the apparatus were lacking. Although some liberties were taken in the construction of the apparatus, the apparatus was used to produce paint stripes with drop-on glass beads. Specifically, the bead dropper mechanism was constructed so that the beads would drop straight down through the mesh box without any rolling movement. The mesh layers were installed in alternating ninety and forty-five degree orientations, which were not specified in the apparatus specifications. Finally, instead of evaluating the embedment of the beads visually, image analysis was used to quantify the percent embedment of a sample of beads on each stripe sample.

The beads used in this experiment were of uniform sizes. However, typical bead mixes have a gradation of bead sizes. The sample production could be used with a normal bead mix, but the image analysis, as it is now would not be able to tell which beads are physical bigger or smaller than the others. As each bead changes in size, the beads exposed diameter would produce a different percentage embedment. Future work into the refinement of the image analysis could allow typical bead mixes to be used on the stripes rather than uniformly sized beads.

## References


[1] Rasdorf, W. J., Hummer, J. E., Zhang, G., & Sitzabee, W. E., *Pavement Marking Performance Analysis*. North Carolina Department of Transportation, Raleigh, NC, 2009

[2] Migletz, J. and Graham, J., Long-term Pavement Marking Practices. NCHRP Synthesis 306, Transportation Research Board, Washington D.C., 2002

[3] Hollingsworth, J. *Understanding the Impact of Bead Type on Paint and Thermoplastic Pavement Markings*, Air Force Institute of Technology, 2012

[4] Texas Department of Transportation. *Pavement Marking Handbook.* Texas, 2004

[5] Austin, R., Schultz, R. *Guide to Retroreflection Safety Principles and Retroreflective Measurements*. RoadVista, San Diego, CA, ISBN 0-9710215-0-3, 2009

[6] *Manual on Uniform Traffic Control Devices*. Federal Highway Administration, Washington D.C., 2009

[7] *Standard Test Method for Measurement of Retroreflective Pavement Marking Materials with CEN-Prescribed Geometry Using a Portable Retroreflectometer.* ASTM E1710 Book of Standard Volume 06.01, 2005

[8] Abbas, A. *Nighttime Visibility of 3M AWP and 3M 380WR ES Durable Tape Under Dry, Wet, and Rainy Conditions.* Report No. FHWA/OH-2012/6, University of Akron, Ohio Department of Transportation, 2012

[9] Delta, *Reflection and Retroreflection,* Technical Note RS 101, http://www.madebydelta.com/imported/images/documents/Roadsensors/RS101.pdf , Last Accessed 4/7/2014

[10] Bahar, G. et al. *NCHRP Web-Only Document 92: Pavement Marking Materials and Markers: Real-World Relationship Between Retroreflectivity and Safety Over Time.* Transportation Research Board, 2006

[11] Stoudt, M., Vedam, K. *Retroreflection from Spherical Glass Beads in Highway Pavement Markings. 1: Specular Reflection.* Applied Optics, Vol. 17, No.12, 1978

[12] Stoudt, M., Vedam, K. *Retroreflection from Spherical Glass Beads in Highway Pavement Markings. 2: Diffuse Reflection (A First Approximation Calculation).* Applied Optics, Vol. 17, No.12, 1978

[13] Grosges, T. *Retro-reflection of Glass Beads for Traffic Road Stripe Paints.* Optical Materials, Vol. 30, p1549-1554, Elsevier, 2007

[14] Boulanger, R., Carlson, P., Fatkin, H,. and AdityaRaut-Desai, A., *Screening Level Assessment of Arsenic and Lead Concentrations in Glass Beads Used in Pavement Markings.* FHWA-HRT-14-021, Research, Development, and Technology Turner-Fairbank Highway Research Center, McLean, VA, 2014

[15] Ozelim, L. and Turochy, R. *Modeling Retroreflectivity Performance of Thermoplastic Pavement Markings in Alabama,* Journal of Transportation Engineering, 10.1061/(ASCE)TE.1943-5436.0000661 , 05014001, 2014

[16] Dale, Mark R. T., *Spatial Pattern Analysis in Plant Ecology*. Cambridge University Press, 1999

[17] Thamizharasan, A., Sarasura, W., Clarke, D., *A Methodology for Estimating the Lifecycle of Interstate Highway Pavement Marking Retroreflectivity.* TRB Paper Number: 03-3867, Washington, D.C., 83rd Transportation Research Board Annual Meeting, 2003

[18] Smadi, O. et al. *NCHRP Report 743: Predicting the Initial Retroreflectivity of Pavement markings from Glass Bead Quality.* Transportation Research Board, Washington D.C., 2013

[19] ADOT, *Standard Specifications for Road And Bridge Construction* ,Phoenix, AZ, 2008

# APPENDIX A

# SAMPLE PREPARATION PROCEDURE

Preparation of Glass Substrate

1. If re-using a glass substrate from a previous sample, ensure that the glass substrate is clean. Most water based paints can be removed with warm water and scrubbing with a sponge or paper towel.
2. Ensure that glass substrate is dry before placement into base of apparatus.

Set up Beads in Drop Box Apparatus

3. Ensure that the hopper on top of the drop box is closed and secure.
4. Turn on the balance
5. Place a clean container on the balance and set to zero
6. Place the desired mass of glass beads into the container
7. Monitor the mass and add or remove the beads from the container until the desired mass is reached
8. Transfer the beads from the container into the hopper by carefully and as evenly as possible pouring the beads into the hopper
9. Use a clean paint stirrer or flathead screwdriver to evenly spread the bead the length of the hopper
10. Use the horizontal lines etched into the inside of the hopper as a guide to ensure the beads are as evenly distributed as possible.
11. Tapping the sides of the hopper can help the beads settle in the hopper evenly
12. Record the mass of beads used on the sample and the application rate

Set up Base

13. Prepare the countertop by covering it with newspaper

14. Place the base on the counter so that the paint application will go from right to left
15. Place glass substrate on the base by inserting it under the lips provided by the plywood strips on the top of the base

Prepare Drawdown Blade and Wet Film Thickness Comb

16. Ensure that the drawdown blade is clean and dry
17. Place the drawdown blade so that the desired opening is facing downward and on the right edge of the glass substrate
18. Record the drawdown blade gap used for the sample

Prepare Paint

19. Carefully shake paint can
20. Open paint can
21. Thoroughly stir the paint with a wooden paint stirrer
22. Once thoroughly stirred, pour the paint into a small container such as a small paint tray

Prepare Rinsing Bowl

23. Prepare a bowl with clean, warm water.
24. Place the bowl near your work station

Sample Production

25. Pour paint into the center of the drawdown blade
26. Move the blade across the stripe from left to right
27. Allow excess paint to fall off the edge of the glass substrate
28. Place drawdown blade into the rinsing bowl

29. Move the base away from the pool of excess paint
30. Within 20 seconds complete the following:
    .30.1. Move the drop box into position on top of the base so that the bars on the side of the drop box align with the ends of the base
    .30.2. Unlock the hopper by loosening the rods in the top
    .30.3. Squeeze the top plates of the hopper so that the bottom opens and the glass beads fall through the drop box
31. Remove the drop box and place on the counter out of the way
32. Take a measurement with the wet film thickness comb as close to the area of striping with beads. Ensure that the comb is penetrating the paint all the way to the glass substrate without touching any glass beads
33. Place the wet film thickness comb into the rinsing bowl
34. Record the wet film thickness measurement
35. Allow Sample to Dry Overnight

Cleaning of Equipment

36. Take the rinsing bowl to a sink
37. Thoroughly clean all paint off of the drawdown blade and wet film thickness comb. Most of the paint will come off with warm water and soap.
38. Empty the dirty water from the mixing bowl.
39. Dry the drawdown blade and wet film thickness comb
40. Carefully close and seal the paint can
41. Wash any other utensils and containers

Once sample is dry

42. Gently brush off any beads that have not adhered to the paint
43. Label the sample with a marker of a piece of duct tape on the bottom of the sample near one edge

Prepare Sample for Image Analysis

44. On the 24″ edges of the glass substrate place a piece of clear tape on the edge so that a mark can be drawn at 12″.
45. Use a thin marker to mark the 12″ point on both sides of the glass.
46. From each 12″ mark, place a piece of tape 10 cm away on both sides of the mark and mark the 10cm distance. This defines the 20 cm length of the measurement area of the retroreflectometer.
47. Place two pieces of duct tape across the sample at the 10 cm marks so that the center 20 cm of the stripe are not covered by the tape.
48. On the duct tape, measure 3″ from the edge to define the center of the stripe
49. From the 3″ measure 2.25 cm on either side and place a mark on the duct tape. This defines the 4.5 cm width of the measurement area
50. Repeat this for the other piece of duct tape
51. Place two pieces of duct tape along the 2.25 cm marks so that the central 4.5cm x 20cm area of the stripe is exposed
52. On the pieces of duct tape extend the 12″ centerline by connecting the 12″ marks drawn earlier. DO NOT DRAW THE LINE OVER THE SAMPLE
53. On a piece of the duct tape, draw an arrow indicating the direction of paint application.
54. Label the sample on a piece of duct tape

# APPENDIX B

# IMAGE ANALYSIS PROCEDURES

Obtaining Overhead Images

1. For overhead images use a flatbed scanner capable of obtaining 2400ppi resolution.
2. Turn on the scanner and place the sample so that the side of the stripe with beads will be scanned.
3. For samples with big beads, use a scan resolution of 1200 ppi. For samples with small beads use a scan resolution of 2400 ppi.
4. Run a preview scan.
5. Depending on the scanner software, crop the preview scan so that the entire exposed central area will be scanned along with some of the duct tape.
6. Scan the image
7. Save the image
8. Examine the image to ensure it is not blurry and no errors were encountered during the scan

Obtaining Side View Images

9. For side view images use the base of the drop box apparatus to prop up one edge of the sample. The height of the base was 38.5 mm.
10. Mark the duct tape near the exposed bead area in order to divide the area into thirds
11. Place the sample so that one edge rests on the edge of the base and the other rests on the counter surface. The height of the counter was 36 and 7/16 ″ high.
12. Place the base of the apparatus so that it is 16cm from the edge of the counter

13. Set up the camera on a tripod so that the viewfinder captures the center of the measurement area. In this case the bottom of the camera clip was 89.5 cm from the floor.
14. Move the sample so that the first third is captured in the viewfinder.
15. Adjust the focus so that the nearest bead appear to be in focus
16. Take the picture
17. Readjust the focus so that a band of beads further away on the sample comes into focus
18. Take the picture
19. Move the sample so that the next third of the measurement area is within the viewfinder.
20. Repeat the process of adjusting the focus and taking picture until images of all three thirds of the measurement area have been obtained.
21. Save pictures to a computer
22. Examine the pictures to ensure that two bands of beads are in focus.
23. Take additional/replacement pictures as necessary

Image Analysis – Overhead Counting Beads

1. Open the image in *ImageJ* by clicking *File* > *Open* and selecting the desired file
2. Change the image to RBG color by clicking *Image* > *Type* > *RBG Color*
3. Change the image to a 16 bit image by clicking *Image* > *Type* > *16-bit*
4. Set the image scale by clicking *Analyze* > *Set Scale*
5. In the dialog box ensure that the 'Distance in pixels' field match the resolution at which the image was scanned
6. In the 'Known distance' field enter 25.4
7. In the 'Unit of Length' field enter 'mm'
8. Click *OK* to close the dialog box
9. Adjust image threshold by clicking *Image* > *Adjust* > *Threshold*
10. Adjust the slider until it appears that all the beads are being captured in the binary image. Try a range from approximately 80-200
11. Close the threshold dialog box
12. Using the rectangular or polygon selection tool, draw a box around the area of the image with beads
13. Clear the rest of the image by clicking *Edit* > *Clear Outside*
14. Despeckle the image by clicking *Process* > *Nosie* > *Despeckle*
15. Repeat the Despeckle two more times
16. Convert the image to a binary image by clicking *Process* > *Binary* > *Make Binary*
17. Click *Process* > *Binary* > *Open*
18. Click *Process* > *Binary* > *Fill Holes*

19. Click *Process* > *Binary* > *Watershed*
20. Click *Analyze* > *Analyze Particles*
21. In the dialog box:
    .21.1. Size: about 1/10 of the expected area to twice the expected diameter
    .21.2. Circularity 0-1
    .21.3. Show: Ellipses
    .21.4. Check boxes: display results, Summarize, exclude on edges, include holes
22. Click *OK*
23. Three new windows will open: 'Summary' displays a summary of the counted particles, 'Results' shows specific measurements, 'Drawing of…' displays an image of the ellipses of the counted particles
24. On the primary *ImageJ* command window open the original image
25. Click the 'Drawing of…' window to make it active
26. Click *Image* > *Overlay* > *Add Image*
27. Select the original image from the drop down list, leave the X location and Y location equal to zero and set the opacity to 75%
28. The overlay image will allow you to see how well or poorly the thresholding worked
29. The overlay can be removed by clicking *Image* > *Overlay* > *Remove Overlay*
30. Adjust the parameters such as size and circularity in the 'Analyze Particles' dialog box until satisfied with the particle counting
31. If necessary, repeat the entire process from the beginning and adjust the threshold values in order to count as many particles as possible

32. Save the ‘Drawing of…’ image as a Tiff and save the results file as a text file

Image Analysis – Overhead Exposed Diameter Measurement

1. Open the image in *ImageJ* by clicking *File* > *Open* and selecting the desired file
2. Set the image scale by clicking *Analyze* > *Set Scale*
3. In the dialog box ensure that the ‘Distance in pixels’ field match the resolution at which the image was scanned
4. In the ‘Known distance’ field enter 25.4
5. In the ‘Unit of Length’ field enter ‘mm’
6. Click *OK* to close the dialog box
7. Using the cursor, determine the minimum and maximum x, y coordinates
8. In *EXCEL* record the minimum and maximum x, y coordinates
9. Use *EXCEL* function *Randbetween* to generate thirty random x, y coordinate pairs between the minimum x and y values
10. Copy the randomly generated coordinates and paste in the same position as ‘values’
11. Find the first x, y coordinate pair in the image by moving the cursor and looking at the displayed x and y position in the main window of *ImageJ*.
12. Determine if a bead is present at the coordinates
13. If no bead is present, find the nearest bead by clicking and dragging the cursor to the center of the nearest bead. The length of the line is displayed in the main window of *ImageJ*
14. When a bead has been located, zoom into the image to 300%

15. Measure the x-diameter by clicking and dragging horizontally across the bead while holding the ‘Shift’ key. The distance will be displayed in the main window of *ImageJ*.
16. Record the x-diameter in *EXCEL*
17. Measure the y-diameter by clicking and dragging vertically across the bead while holding the ‘Shift’ key. The distance will be displayed in the main window of *ImageJ*.
18. Record the y-diamter in *EXCEL*
19. Repeat steps 12-17 for the remaining randomly generated coordinates
20. In *EXCEL,* take average the x-diameter and y-diameter for each coordinate pair to obtain the average exposed diameter
21. Record the average diameter of each bead

Image Analysis – Side Angle View Meausrements

1. In *ImageJ*, open the desired image
2. Use the line tool to measure the bead diameter
3. Record the value in *EXCEL*
4. Use the line tool to measure the distance from the paint to the top of the bead
5. Record the value in *EXCEL*
6. Repeat Steps 1-6 for all six images for a single striping sample

# APPENDIX C

# EQUATIONS

## Big Bead Partial Spherical Volume

| Volume of a Sphere | | |
|---|---|---|
| V= | 0.54 | mm^3 |
| D= | 1.01 | mm |
| r= | 0.51 | mm |

| Volume of Partial Sphere | | 40 |
|---|---|---|
| h= | 0.438 | mm |
| r= | 0.506 | mm |
| c= | 0.501 | mm |
| V= | 0.217 | mm^3 |
| Target Volume | Difference | |
| 0.217 | 0.000 | mm^3 |

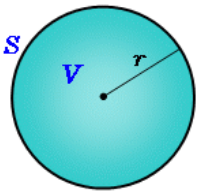


*Sphere*

(1) *volume:* $V=\frac{4}{3}\pi r^3$

(2) *surface area:* $S=4\pi r^2$

| Volume of Partial Sphere | | 60.000 |
|---|---|---|
| h= | 0.573 | mm |
| r= | 0.506 | mm |
| c= | 0.501 | mm |
| V= | 0.325 | mm^3 |
| Target Volume | Difference | |
| 0.325 | 0.000 | mm^3 |

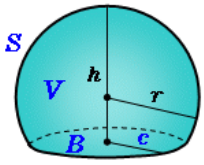


*Partial sphere*

(1) *radius of bottom:* $c=\sqrt{h(2r-h)}$

(2) *volume:* $V=\frac{\pi}{6}h(3c^2+h^2)$

(3) *surface area:* $S=\pi(c^2+h^2)=2\pi rh$ *exclude* $B$

(4) *base area:* $B=\pi c^2$

## Small Bead Partial Spherical Volume

| Volume of a Sphere | | |
|---|---|---|
| V= | 0.046 | mm^3 |
| D= | 0.445 | mm |
| r= | 0.223 | mm |

| Volume of Partial Sphere (50% Exposed) | | |
|---|---|---|
| h= | 0.429 | mm |
| r= | 0.223 | mm |
| c= | 0.084 | mm |
| V= | 0.046 | mm^3 |
| Target Volume | Difference | |
| 0.046 | 0.000 | mm^3 |

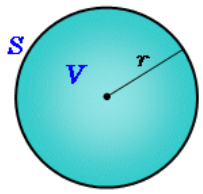


*Sphere*

(1) *volume:* $V=\frac{4}{3}\pi r^3$

(2) *surface area:* $S=4\pi r^2$

| Volume of Partial Sphere (50% Embedded) | | |
|---|---|---|
| h= | 0.016 | mm |
| r= | 0.223 | mm |
| c= | 0.084 | mm |
| V= | 0.000 | mm^3 |
| Target Volume | Difference | |
| 0.000 | 0.000 | mm^3 |

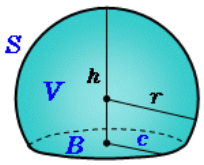


*Partial sphere*

(1) *radius of bottom:* $c=\sqrt{h(2r-h)}$

(2) *volume:* $V=\frac{\pi}{6}h(3c^2+h^2)$

(3) *surface area:* $S=\pi(c^2+h^2)=2\pi rh$ *exclude* $B$

(4) *base area:* $B=\pi c^2$

Big Bead % Embedment Calculation>50%

$$\%\,\text{Embedment} = 92826.555 * Diameter - 850839.972 * D^2 + 4064402.661 * D^3$$
$$-10681066.052 * D^4 + 14656633.180 * D^5 - 8218785.635 * \text{D}^6 - 4021.265$$

Where *D* is the average exposed diameter of the bead

Small Bead % Embedment Calculation>50%

$$\%Embedment = 41548.450 * D - 439901.427 * D^2 + 2388156.071 * D^3$$
$$-7057856.682 * D^4 + 10815247.382 * D^5 - 6742593.976 * \text{D}^6 - 1456.938$$

Where *D* is the average exposed diameter of the bead

MatLab Algorithm for Nearest Neighbor Distance

[IDX, D]=knnsearch (C,C,'K',2,'Distance','Euclidean')

Where C is a matrix with x,y corrdinates

Matrix IDX equals the index of the nearest neighbor

Matrix D equals the nearest neighbor distance

Matlab Function for X Direction Nearest Neighbor

```
clc
clear all
data=xlsread('PS06_NN_dist.xls');
x = data(:,1);
y = data(:,2);
dist_nn = data(:,3);
mat_len = size(x,1);

for i = 1:mat_len
    temp_x = x(i,:);
    temp_y = y(i,:);
    ulim_y = temp_y + 0.415;
    llim_y = temp_y -0.415;
    k = 1;
    temp_mat_y = [];
    for j = 1:mat_len;

      %  if (y(j,:) == temp_y)
       %     k = k-1;
      %  end

        if (y(j,:) ~= temp_y) & (y(j,:) <= ulim_y) & (y(j,:) >= llim_y)
            temp_mat_y(k,:) = y(j,:);
            temp_mat_x(k,:) = x(j,:);
            temp_loc_(k,:)=j;
        else
            k=k-1;
        end
        k = k+1;
    end
    search_len = size(temp_mat_y,1);
    diff_x = [];
    for p = 1:search_len
        diff_x(p,:) = abs(temp_x - temp_mat_x(p,:));
    end
    x_nn(i,:) = min(diff_x);
end
data(:,4) = x_nn(:,1);
```

# APPENDIX D

## DATA SHEETS

| Sample | Bead size | Application Rate (lb/gal) | Bead Mass(g) | Central area bead count | Retroreflectivity | %Embedment | VTMR | NN dist | XNN |
|---|---|---|---|---|---|---|---|---|---|
| PB14 | -16+22 | 1.5 | 3.25 | 409 | 87 | 27.06 | 0.69 | 2.44 | 5.81 |
| PB09 | -16+20 | 1.5 | 3.25 | 401 | 293 | 73.91 | 1.27 | 2.27 | 5.23 |
| PB10 | -16+20 | 1.5 | 3.25 | 429 | 249 | 85.85 | 1.00 | 2.52 | 6.03 |
| PB13 | -16+21 | 3 | 6.5 | 839 | 160 | 25.26 | 0.63 | 1.88 | 3.28 |
| PB16 | -16+20 | 3 | 6.5 | 918 | 420 | 61.20 | 2.77 | 1.75 | 2.63 |
| PB07 | -16+20 | 3 | 6.5 | 815 | 601 | 67.60 | 1.16 | 1.84 | 3.13 |
| PB08 | -16+20 | 3 | 6.5 | 801 | 457 | 81.41 | 1.33 | 1.80 | 3.25 |
| PB04 | -16+20 | 6 | 13 | 1692 | 375 | 34.12 | 2.35 | 1.38 | 1.62 |
| PB01 | -16+20 | 6 | 13 | 1663 | 442 | 36.66 | 1.21 | 1.41 | 1.61 |
| PB02 | -16+20 | 6 | 13 | 1575 | 508 | 67.98 | 1.73 | 1.43 | 1.63 |
| PB03 | -16+20 | 6 | 13 | 1647 | 609 | 68.73 | 1.65 | 1.41 | 1.70 |
| PB06 | -16+20 | 6 | 13 | 1607 | 549 | 83.80 | 1.65 | 1.40 | 3.06 |
| PB05 | -16+20 | 6 | 13 | 1702 | 519 | 84.04 | 3.59 | 1.37 | 3.01 |
| PB15 | -16+23 | 12 | 26 | 3408 | 178 | 28.00 | 1.07 | 1.05 | 0.90 |
| PB12 | -16+20 | 12 | 26 | 3447 | 330 | 76.18 | 0.71 | 1.11 | 0.90 |
| PB17 | -16+20 | 12 | 26 | 3028 | 194 | 35.00 | 2.01 | 1.14 | 0.90 |
| PB18 | -16+20 | 12 | 26 | 3319 | 378 | 68.78 | 1.67 | 1.30 | 0.96 |
| PB11 | -16+20 | 12 | 26 | 3459 | 450 | 83.47 | 1.83 | 1.12 | 0.95 |

| PB01 | |
|---|---|
| Bead Used | -16+20 |
| Application Rate(lb/gal) | 6 |
| Drawdown blade opening (mil) | 20 |
| Bead Mass(g) | 13.00 |
| **Measured - Central Area** | |
| Exposed diameter (mm) | 1.03 |
| Retroreflectivity | 442 |
| Bead Count | 1663.00 |
| **Calculated** | |
| %embedment | 1116 |
| VTMR | 1.20902 |
| Nearest Neighbor dist(mm) | 1.410104 |
| XNN (mm) | 8.80 |

| PB02 | |
|---|---|
| Bead Used | -16+20 |
| Application Rate(lb/gal) | 6 |
| Drawdown blade opening (mil) | 20 |
| Bead Mass(g) | 13.00 |
| **Measured - Central Area** | |
| Exposed diameter (mm) | 0.98 |
| Retroreflectivity | 508 |
| Bead Count | 1575.00 |
| **Calculated** | |
| %embedment | 67.98 |
| VTMR | 1.73 |
| Nearest Neighbor dist(mm) | 1.43 |
| XNN (mm) | 1.63 |

| PB03 | |
|---|---|
| Bead Used | -16+20 |
| Application Rate(lb/gal) | 6 |
| Drawdown blade opening (mil) | 25 |
| Bead Mass(g) | 13.00 |
| **Measured - Central Area** | |
| Exposed diameter (mm) | 0.97 |
| Retroreflectivity | 609 |
| Bead Count | 1647.00 |
| **Calculated** | |
| %embedment | 68.73 |
| VTMR | 1.65 |
| Nearest Neighbor dist(mm) | 1.41 |
| XNN (mm) | 1.70 |

| PB04 | |
|---|---|
| Bead Used | -16+20 |
| Application Rate(lb/gal) | 6 |
| Drawdown blade opening (mil) | 20 |
| Bead Mass(g) | 13.00 |
| **Measured - Central Area** | |
| Exposed diameter (mm) | 30.52 |
| Retroreflectivity | 375 |
| Bead Count | 1692.00 |
| **Calculated** | |
| %embedment | 34.12 |
| VTMR | 2.35 |
| Nearest Neighbor dist(mm) | 1.38 |
| XNN (mm) | 1.62 |

| PB05 | |
|---|---|
| Bead Used | -16+20 |
| Application Rate(lb/gal) | 6 |
| Drawdown blade opening (mil) | 30 |
| Bead Mass(g) | 13.00 |
| **Measured - Central Area** | |
| Exposed diameter (mm) | 0.90 |
| Retroreflectivity | 519 |
| Bead Count | 1702.00 |
| **Calculated** | |
| %embedment | 84.04 |
| VTMR | 3.59 |
| Nearest Neighbor dist(mm) | 1.37 |
| XNN (mm) | 3.01 |

| PB06 | |
|---|---|
| Bead Used | -16+20 |
| Application Rate(lb/gal) | 6 |
| Drawdown blade opening (mil) | 30 |
| Bead Mass(g) | 13.00 |
| **Measured - Central Area** | |
| Exposed diameter (mm) | 0.90 |
| Retroreflectivity | 549.3333 |
| Bead Count | 1607.00 |
| **Calculated** | |
| %embedment | 83.80 |
| VTMR | 1.65 |
| Nearest Neighbor dist(mm) | 1.40 |
| XNN (mm) | 3.06 |

| PB07 | |
|---|---|
| Bead Used | - 16+20 |
| Application Rate(lb/gal) | 3 |
| Drawdown blade opening (mil) | 25 |
| Bead Mass(g) | 6.50 |
| **Measured - Central Area** | |
| Exposed diameter (mm) | 0.98 |
| Retroreflectivity | 601 |
| Bead Count | 815.00 |
| **Calculated** | |
| %embedment | 67.60 |
| VTMR | 1.16 |
| Nearest Neighbor dist(mm) | 1.84 |
| XNN (mm) | 3.13 |

| PB08 | |
|---|---|
| Bead Used | - 16+20 |
| Application Rate(lb/gal) | 3 |
| Drawdown blade opening (mil) | 30 |
| Bead Mass(g) | 6.50 |
| **Measured - Central Area** | |
| Exposed diameter (mm) | 0.92 |
| Retroreflectivity | 457 |
| Bead Count | 801.00 |
| **Calculated** | |
| %embedment | 81.41 |
| VTMR | 1.33 |
| Nearest Neighbor dist(mm) | 1.80 |
| XNN (mm) | 3.25 |

| PB09 | |
|---|---|
| | - |
| Bead Used | 16+20 |
| Application Rate(lb/gal) | 1.5 |
| Drawdown blade opening (mil) | 30 |
| Bead Mass(g) | 3.25 |
| **Measured - Central Area** | |
| Exposed diameter (mm) | 0.95 |
| Retroreflectivity | 293 |
| Bead Count | 401.00 |
| **Calculated** | |
| %embedment | 73.91 |
| VTMR | 1.27 |
| Nearest Neighbor dist(mm) | 2.27 |
| XNN (mm) | 5.23 |

| PB10 | |
|---|---|
| Bead Used | -16+20 |
| Application Rate(lb/gal) | 1.5 |
| Drawdown blade opening (mil) | 40 |
| Bead Mass(g) | 3.25 |
| **Measured - Central Area** | |
| Exposed diameter (mm) | 0.88 |
| Retroreflectivity | 248.6667 |
| Bead Count | 429.00 |
| **Calculated** | |
| %embedment | 85.85 |
| VTMR | 1.00 |
| Nearest Neighbor dist(mm) | 2.52 |
| XNN (mm) | 6.03 |

| PB11 | |
|---|---|
| Bead Used | -16+20 |
| Application Rate(lb/gal) | 12 |
| Drawdown blade opening (mil) | 30 |
| Bead Mass(g) | 26.00 |
| **Measured - Central Area** | |
| Exposed diameter (mm) | 0.90 |
| Retroreflectivity | 449.6667 |
| Bead Count | 3459.00 |
| **Calculated** | |
| %embedment | 83.47 |
| VTMR | 1.83 |
| Nearest Neighbor dist(mm) | 1.12 |
| XNN (mm) | 0.95 |

| PB12 | |
|---|---|
| Bead Used | -16+20 |
| Application Rate(lb/gal) | 12 |
| Drawdown blade opening (mil) | 20 |
| Bead Mass(g) | 26.00 |
| **Measured - Central Area** | |
| Exposed diameter (mm) | 0.95 |
| Retroreflectivity | 329.6667 |
| Bead Count | 3447.00 |
| **Calculated** | |
| %embedment | 76.18 |
| VTMR | 0.71 |
| Nearest Neighbor dist(mm) | 1.11 |
| XNN (mm) | 0.90 |

| PB013 | |
|---|---|
| Bead Used | -16+20 |
| Application Rate(lb/gal) | 3 |
| Drawdown blade opening (mil) | 15 |
| Bead Mass(g) | 6.50 |
| **Measured - Central Area** | |
| Exposed diameter (mm) | 27.78 |
| Retroreflectivity | 160.3333 |
| Bead Count | 839.00 |
| **Calculated** | |
| %embedment | 25.26 |
| VTMR | 0.63 |
| Nearest Neighbor dist(mm) | 1.88 |
| XNN (mm) | 3.28 |

| PB14 | |
|---|---|
| Bead Used | -16+20 |
| Application Rate(lb/gal) | 1.5 |
| Drawdown blade opening (mil) | 15 |
| Bead Mass(g) | 3.25 |
| **Measured - Central Area** | |
| Exposed diameter (mm) | 32.36 |
| Retroreflectivity | 87 |
| Bead Count | 409.00 |
| **Calculated** | |
| %embedment | 27.06 |
| VTMR | 0.69 |
| Nearest Neighbor dist(mm) | 2.44 |
| XNN (mm) | 5.81 |

| PB15 | |
|---|---|
| Bead Used | -16+20 |
| Application Rate(lb/gal) | 12 |
| Drawdown blade opening (mil) | 15 |
| Bead Mass(g) | 26.00 |
| **Measured - Central Area** | |
| Exposed diameter (mm) | 30.43 |
| Retroreflectivity | 177.6667 |
| Bead Count | 3408.00 |
| **Calculated** | |
| %embedment | 28.00 |
| VTMR | 1.07 |
| Nearest Neighbor dist(mm) | 1.05 |
| XNN (mm) | 0.90 |

| PB16 | |
|---|---|
| Bead Used | -16+20 |
| Application Rate(lb/gal) | 3 |
| Drawdown blade opening (mil) | 20 |
| Bead Mass(g) | 6.50 |
| **Measured - Central Area** | |
| Exposed diameter (mm) | 1.17 |
| Retroreflectivity | 420 |
| Bead Count | 918.00 |
| **Calculated** | |
| %embedment | 61.20 |
| VTMR | 2.77 |
| Nearest Neighbor dist(mm) | 1.75 |
| XNN (mm) | 2.63 |

| PB17 | |
|---|---|
| Bead Used | -16+20 |
| Application Rate(lb/gal) | 12 |
| Drawdown blade opening (mil) | 15 |
| Bead Mass(g) | 26.00 |
| **Measured - Central Area** | |
| Exposed diameter (mm) | 26.49 |
| Retroreflectivity | 194.3333 |
| Bead Count | 3028.00 |
| **Calculated** | |
| %embedment | 29.88 |
| VTMR | 2.01 |
| Nearest Neighbor dist(mm) | 1.14 |
| XNN (mm) | 0.90 |

| PB18 | |
|---|---|
| Bead Used | -16+20 |
| Application Rate(lb/gal) | 12 |
| Drawdown blade opening (mil) | 15 |
| Bead Mass(g) | 26.00 |
| **Measured - Central Area** | |
| Exposed diameter (mm) | 0.97 |
| Retroreflectivity | 378 |
| Bead Count | 3319.00 |
| **Calculated** | |
| %embedment | 68.78 |
| VTMR | 1.67 |
| Nearest Neighbor dist(mm) | 1.30 |
| XNN (mm) | 0.96 |

| PS01 | |
|---|---|
| Bead Used | -30+40 |
| Application Rate(lb/gal) | 6 |
| Drawdown blade opening (mil) | 5 |
| Bead Mass(g) | 13.00 |
| **Measured - Central Area** | |
| Exposed diameter (mm) | 0.37 |
| Retroreflectivity | 212.6667 |
| Bead Count | 33418.00 |
| **Calculated** | |
| %embedment | 86.48 |
| VTMR | 23.39 |
| Nearest Neighbor dist(mm) | 0.32 |
| XNN (mm) | 0.17 |

| PS02 | |
|---|---|
| Bead Used | -30+40 |
| Application Rate(lb/gal) | 3 |
| Drawdown blade opening (mil) | 5 |
| Bead Mass(g) | 6.50 |
| **Measured - Central Area** | |
| Exposed diameter (mm) | 0.39 |
| Retroreflectivity | 343.3333 |
| Bead Count | 15752.00 |
| **Calculated** | |
| %embedment | __z |
| VTMR | __ |
| Nearest Neighbor dist(mm) | 0.43 |
| XNN (mm) | 0.37 |

| PS03 | |
|---|---|
| Bead Used | -30+40 |
| Application Rate(lb/gal) | 1.5 |
| Drawdown blade opening (mil) | 5 |
| Bead Mass(g) | 3.25 |
| **Measured - Central Area** | |
| Exposed diameter (mm) | 0.40 |
| Retroreflectivity | 329.3333 |
| Bead Count | 8381.00 |
| **Calculated** | |
| %embedment | 67.61 |
| VTMR | — |
| Nearest Neighbor dist(mm) | 0.57 |
| XNN (mm) | 0.57 |

| PS04 | |
|---|---|
| Bead Used | -30+40 |
| Application Rate(lb/gal) | 6 |
| Drawdown blade opening (mil) | 10 |
| Bead Mass(g) | 13.00 |
| **Measured - Central Area** | |
| Exposed diameter (mm) | 0.34 |
| Retroreflectivity | 360.6667 |
| Bead Count | 29449.00 |
| **Calculated** | |
| %embedment | 83.60 |
| VTMR | — |
| Nearest Neighbor dist(mm) | 0.39 |
| XNN (mm) | 0.23 |

| PS05 | |
|---|---|
| Bead Used | - 30+40 |
| Application Rate(lb/gal) | 3 |
| Drawdown blade opening (mil) | 5 |
| Bead Mass(g) | 13.00 |
| **Measured - Central Area** | |
| Exposed diameter (mm) | 0.32 |
| Retroreflectivity | 453 |
| Bead Count | 0.00 |
| **Calculated** | |
| %embedment | 88.05 |
| VTMR | — |
| Nearest Neighbor dist(mm) | 0.50 |
| XNN (mm) | 0.48 |

| PS06 | |
|---|---|
| Bead Used | -30+40 |
| Application Rate(lb/gal) | 1.5 |
| Drawdown blade opening (mil) | 5 |
| Bead Mass(g) | 3.25 |
| **Measured - Central Area** | |
| Exposed diameter (mm) | 0.33 |
| Retroreflectivity | 448.3333 |
| Bead Count | 9227.00 |
| **Calculated** | |
| %embedment | 86.95 |
| VTMR | 89.37 |
| Nearest Neighbor dist(mm) | 0.47 |
| XNN (mm) | 0.51 |

| PS07 | |
|---|---|
| Bead Used | -30+40 |
| Application Rate(lb/gal) | 6 |
| Drawdown blade opening (mil) | 1 |
| Bead Mass(g) | 13.00 |
| **Measured - Central Area** | |
| Exposed diameter (mm) | __ |
| Retroreflectivity | 154.3333 |
| Bead Count | 31196.00 |
| **Calculated** | |
| %embedment | 3.93 |
| VTMR | 4.65 |
| Nearest Neighbor dist(mm) | 0.33 |
| XNN (mm) | 0.18 |

| PS08 | |
|---|---|
| Bead Used | -30+40 |
| Application Rate(lb/gal) | 3 |
| Drawdown blade opening (mil) | 1 |
| Bead Mass(g) | 6.50 |
| **Measured - Central Area** | |
| Exposed diameter (mm) | __ |
| Retroreflectivity | 98 |
| Bead Count | 17635.00 |
| **Calculated** | |
| %embedment | 15.89 |
| VTMR | 4.87 |
| Nearest Neighbor dist(mm) | 0.41 |
| XNN (mm) | .35 |

| PS09 | |
|---|---|
| Bead Used | -30+40 |
| Application Rate(lb/gal) | 1.5 |
| Drawdown blade opening (mil) | 1 |
| Bead Mass(g) | 3.25 |
| **Measured - Central Area** | |
| Exposed diameter (mm) | __ |
| Retroreflectivity | 0 |
| Bead Count | 9277.00 |
| **Calculated** | |
| %embedment | 11.54 |
| VTMR | __ |
| Nearest Neighbor dist(mm) | 0.55 |
| XNN (mm) | .66 |